AGU PUBLICATIONS

Geochemistry, Geophysics, Geosystems

RESEARCH ARTICLE
10.1002/2016GC006728

Key Points:
- Provenance analysis of Late Quaternary glaciomarine sediments from Eastern Ross Sea was performed using three distinct analytical techniques
- McAyeal and Bindschadler Ice Streams catchment area is proposed as source region, with unexposed rock units suggested by detrital data
- AFT data in association with clasts occurrence point out to a localized tectonic-related exhumation of portions of Marie Byrd Land

Supporting Information:
- Supporting Information S1

Correspondence to:
M. Perotti,
perotti2@student.unisi.it;
perottimatteo@gmail.com

Citation:
Perotti, M., B. Andreucci, F. Talarico, M. Zattin, and A. Langone (2017), Multianalytical provenance analysis of Eastern Ross Sea LGM till sediments (Antarctica): Petrography, geochronology, and thermochronology detrital data, *Geochem. Geophys. Geosyst.*, *18*, doi:10.1002/2016GC006728.

Received 10 NOV 2016
Accepted 17 MAY 2017
Accepted article online 30 MAY 2017

Multianalytical provenance analysis of Eastern Ross Sea LGM till sediments (Antarctica): Petrography, geochronology, and thermochronology detrital data

Matteo Perotti[1], Benedetta Andreucci[2], Franco Talarico[1], Massimiliano Zattin[2], and Antonio Langone[3]

[1]Department of Physical Sciences, Earth and Environment, University of Siena, Siena, Italy, [2]Department of Geosciences, University of Padova, Padova, Italy, [3]Consiglio Nazionale della Ricerche-Istituto di Geoscienze e Georisorse, Unità di Pavia, Pavia, Italy

Abstract In order to reveal provenance of detrital sediments supplied by West Antarctic Ice Sheet (WAIS), 19 glaciomarine cores of Last Glacial Maximum age were analyzed from Eastern Ross Sea and Sulzberger Bay. Analytical techniques included petrographic analysis of gravel-sized clasts, geochronology (zircon U-Pb: Zrn-UPb) and thermochronology (apatite fission track: AFT) of sand-sized fractions. Petrographic analysis revealed a similarity with the lithologies presently exposed in western Marie Byrd Land (MBL), with major roles played by low-grade metamorphic rocks and granitoids. Furthermore Zrn-UPb and AFT data allowed to identify the ages of formation and cooling of sedimentary source area, consisting of Cambrian-Precambrian basement (i.e., Swanson Formation in western MBL) which underwent at least two episodes of magma intrusion, migmatization and cooling during Devonian-Carboniferous and Cretaceous-Paleocene times. Scarcity of volcanic clasts in the region of Ross Sea along the front of West Antarctica Ice Streams in association with the occurrence of AFT Oligocene-Pliocene dates suggests a localized tectonic exhumation of portions of MBL, as already documented for the opposite side of West Antarctic Rift System in the Transantarctic Mountains. Furthermore, a Zrn-UPb and AFT population of Late Triassic-Jurassic age indicates the presence of unexposed rocks that formed or metamorphosed at that time in the sedimentary source area, which could be identified in McAyeal Ice Stream and Bindschadler Ice Stream catchment areas.

1. Introduction

Glaciated regions such as Antarctica are often characterized by areas with poor rock exposures, so studies of glacial sediments are crucial in revealing glacier dynamics and providing important information about concealed source rocks.

The Ross Sea, hosting at present an extensive ice shelf, is a key area for studying the ice sheets dynamics of Antarctica as it drains about one third of the Antarctic ice, both from the East Antarctic Ice Sheet (EAIS) and West Antarctic Ice Sheet (WAIS, Figure 1). This embayment was occupied, during the Last Glacial Maximum (LGM), by an ice sheet that grounded in proximity of the continental shelf break, leaving stratigraphic and geomorphological traces on the sea bottom sediments [*Domack et al*., 1999; *Shipp et al*., 1999; *Licht et al*., 1999; *Licht and Andrews*, 2002; *Mosola and Anderson*, 2006]. Soon after the LGM, the grounding line retreated to the current position [*Anderson et al*., 2014].

Information about ice sheet dynamics has been provided by provenance analysis of glaciomarine sediments in the works of *Licht et al*. [2005, 2014], *Licht and Palmer* [2013], and *Farmer et al*. [2006]. Although the above cited studies have been carried out on LGM till fractions from the Eastern Ross Sea, knowledge about the catchment areas of West Antarctic Ice Streams feeding this marine region (i.e., Kamb, Bindschadler, and McAyeal Ice Streams) is not complete. Here we present a multianalytical provenance study of Eastern Ross Sea LGM sediments, based on detrital geochronology, thermochronology, and petrographic techniques.

Provenance studies commonly take advantage of detrital geochronology and thermochronology, as they allow inferences to be made about the location, age, and exhumation history of source terrains.

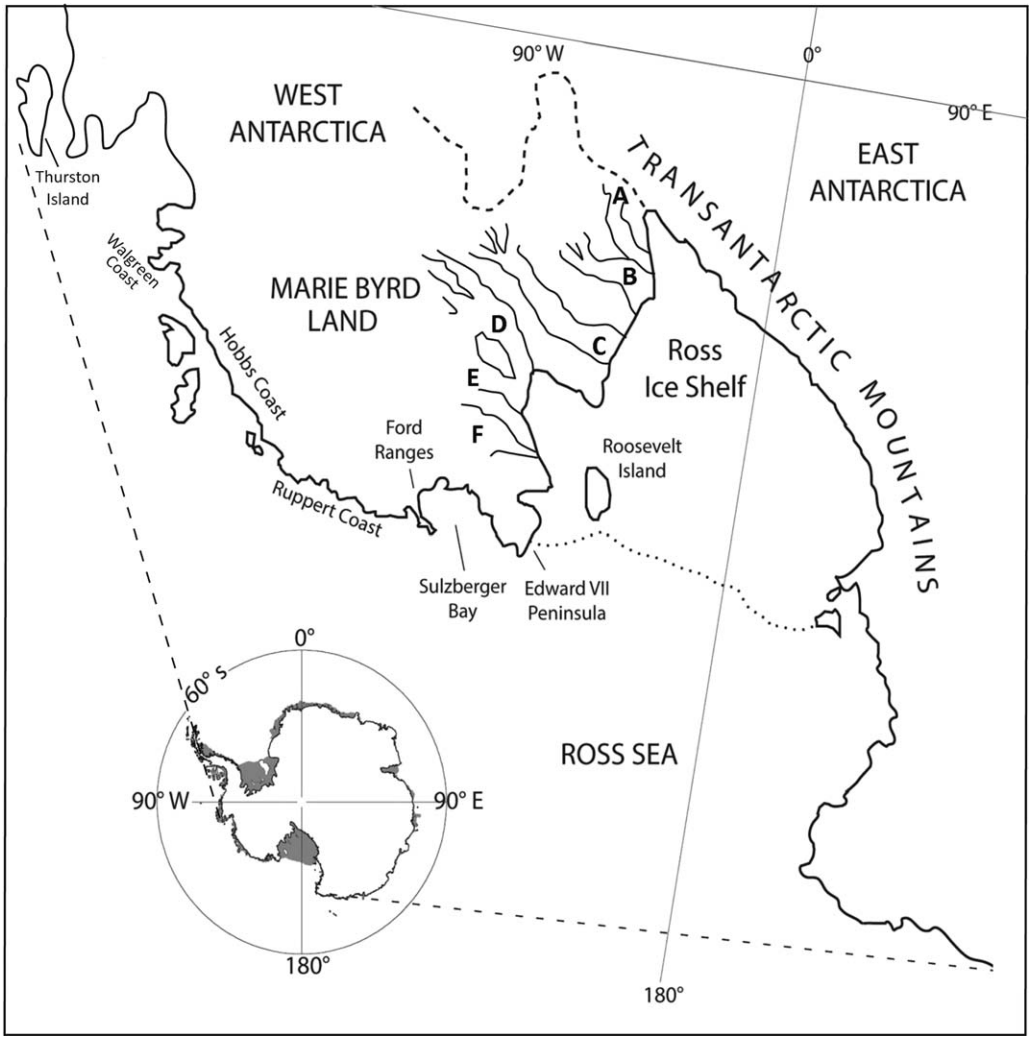

Figure 1. Geographic sketch map of the study area: Eastern Ross Sea and Marie Byrd Land. Also schematic pattern of Siple Coast Ice Streams is shown (labeled A–F: A: Mercer Ice Stream; B: Whillans Ice Stream; C: Kamb Ice Stream; D: Bindschadler Ice Stream; E: MacAyeal Ice Stream; F: Echelmeyer Ice Stream).

Comparison between age populations found in sedimentary samples versus regional bedrock ages allows the identification of possible source areas that may be used to determine ice flow drainage patterns. In addition, petrography of a gravel-sized fraction can give a complete microstructural and lithological picture of the rocks involved in the erosional framework, thus allowing a robust interpretation of geology of the source area. This methodology has been successfully used in Antarctica to track provenance changes and unravel paleo ice-flow patterns evolution through time [e.g., *Talarico and Sandroni*, 2011]. Provenance studies in the Eastern Ross Sea have so far provided petrographic data only from medium and coarse sand fraction analysis [*Anderson et al*., 1992; *Licht et al*., 2005].

In this work, we present a geochronological and thermochronological provenance study of Eastern Ross Sea LGM sediments, combined with a gravel-sized clasts petrographic analysis. The methodology allowed us to identify distinct different eroded source rock units, consisting of metamorphic basement, metasediments, volcanic, and plutonic rocks, and to obtain information about crystallization, metamorphism, and exhumation history of source rock units. The combined data set obtained with this study well matches the western Marie Byrd Land geology, therefore illuminating the ice drainage patterns during LGM.

2. Geological Setting

2.1. Geology of Western Marie Byrd Land

The Ross Sea Embayment is bordered by the 3500 km-long mountain chain of the Transantarctic Mountains to the west and Marie Byrd Land to the east. The modern West Antarctic Ice Sheet occupies part of the West Antarctic Rift System, formed in the mid-Cretaceous to Cenozoic with a total horizontal displacement of several hundreds to thousand kilometers between Marie Byrd Land and East Antarctica [*Di Venere et al*., 1994; *Luyendyk et al*., 2003; *Siddoway*, 2008; *Storti et al*., 2008].

The best exposed rock outcrops in West Antarctica are in Marie Byrd Land. The oldest unit is the Neoproterozoic-Cambrian Swanson Formation [*Bradshaw et al*., 1983; *Adams*, 1986; *Pankhurst et al*., 1998]; it is a folded and cleaved low-grade metaturbidite sequence which has been correlated on the basis of U-Pb detrital zircon ages to the Robertson Bay Group in North Victoria Land and Greenland Group in Western New Zealand [*Adams et al*., 2013; *Ireland et al*., 1998]. It crops out mainly in the Ford Ranges in western Marie Byrd Land. Low-grade-metasedimentary rocks are also exposed in small outcrops in eastern Marie Byrd Land [*Brand*, 1979].

The Swanson Formation was intruded by Devonian-Carboniferous Ford Granodiorite suite, which records a major pulse of calc-alkaline magmatism along the Antarctica-Zealandia-Australia segment of Gondwana continental margin [*Weaver et al*., 1991]. The Ford Granodiorite is a suite of gray to black and white metaluminous to peraluminous I-type biotite-hornblende granodiorites-tonalites [*Weaver et al*., 1991]. Two hypotheses have been proposed for this event: subduction [*Weaver et al*., 1991] or back-arc extension [*Tulloch et al*., 2009]. It is unclear if plutons of Ford Granodiorite were emplaced in Ford Ranges during short-lived pulses or prolonged magmatism during the Devonian-Carboniferous [*Pankhurst et al*., 1998; *Siddoway and Fanning*, 2009; *Yakymchuk et al*., 2015].

The inboard area of a calc-alkaline Jurassic-Cretaceous magmatic arc along the east Gondwana margin was involved in the emplacement of alkaline Byrd Coast Granite suite occurred in Cretaceous time, with ages of 124–95 Ma [*Weaver et al*., 1992]. The Byrd Coast Granite intruded both the Swanson Formation and the Ford Granodiorite suite and chemically derived from the latter in a setting of back-arc extension [*Weaver et al*., 1992] or intracontinental extension [*Korhonen et al*., 2010a, 2010b]. This is a pinkish coarse equigranular to porphyritic A-type leucogranite and monzogranite variety. This igneous activity involved Ruppert and Hobbs Coast (110–101 Ma) [*Mukasa and Dalziel*, 2000] and Ford Ranges-Edward VII Peninsula region [*Weaver et al*., 1992; *Pankhurst et al*., 1998]. Crustal extension in Cretaceous produced also the emplacement of mafic dykes throughout the Ford Ranges [*Siddoway et al*., 2005; *Saito et al*., 2013]. Within the Ford Ranges, a migmatite-granite complex is exposed in the Fosdick Mountains [*Siddoway et al*., 2004a], with orthogneisses and paragneisses which underwent at least two high-grade metamorphic events, in Devonian-Carboniferous and Cretaceous time, respectively [*Korhonen et al*., 2010a, 2010b, 2012; *Yakymchuk et al*., 2015]. The granulite facies gneisses consist of migmatitic paragneisses with discrete domains of melanosome which typically contains cordierite, sillimanite, biotite, quartz, plagioclase, and k-feldspars, with or without garnet, and coarser grained leucosome containing quartz, k-feldspar, anti-perthite, and biotite, with or without garnet [*Korhonen et al*., 2010a, 2010b]. On the other hand, migmatitic orthogneisses are mainly composed by quartz, plagioclase, k-feldspar, biotite, iron oxides and in some cases may contain garnet [*Korhonen et al*., 2010a, 2010b].

Other migmatites are exposed in the Alexandra Mountains (Edward VII Peninsula) [*Smith*, 1996] and in Demas Range, eastern Marie Byrd Land [*Mukasa and Dalziel*, 2000].

The emplacement of youngest components of the Byrd Coast Granite coincides with the onset of regional extension to transtension and to the development of the West Antarctic Rift System [*Siddoway*, 2008].

During the Cenozoic, starting from about 35 Ma, the region was affected by an intense alkaline volcanism and uplift of Marie Byrd Land Dome, which today has an area of 800 $\times$ 500 km and an altitude reaching 2700 m above sea level [*LeMasurier et al*., 2011]. Eighteen major volcanoes and many smaller centers are known in the region and are composed of felsic alkaline lavas (phonolite, trachyte, rhyolite, and intermediate differentiates) [*Panter et al*., 2000]. They are distributed as linear ranges in central Marie Byrd Land, such as the Flood Range and Executive Committee Range. Moreover, several volcanic centers are believed to exist subglacially beneath the WAIS, as demonstrated during the Central West Antarctica aerogeophysical survey carried out from 1991 to 1997 over the region [*Behrendt et al*., 1994, 1996, 2004].

Starting from about Oligocene time [*Ivany et al*., 2006 in Antarctic Peninsula], West Antarctica was involved in the first development of an ice sheet which enlarged further forming the West Antarctic Ice Sheet in Middle to Late Miocene time [*Barker and Camerlenghi*, 2002]. In this scenario, on the basis of geomorphological evidences, Marie Byrd Land was affected since ~15 Ma by a cold-based glaciation [*Rocchi et al*., 2006]. The WAIS collapsed several times during Pliocene [*Naish et al*., 2009; *Pollard and DeConto*, 2009]. Currently, almost one third of the ice of Antarctica is drained to the Ross Sea Embayment, both from the EAIS and the WAIS. EAIS ice flows come from big outlet glaciers through the Transantarctic Mountains, while most of the West Antarctica ice flows from fast moving Ice Streams, without any significant rock exposures. Some of the Ice Streams (Whillans and Mercer Ice Streams) [*Licht et al*., 2014] could drain ice also from the southern sector of the Transantarctic Mountains. The current ice-flow pattern is different from that occurring during last glaciation, according to indicators of flow of overriding ice across some mountain ranges in western Marie Byrd Land during LGM [*Sugden et al*., 2005 for the Ford Ranges]. These authors demonstrated that some regional LGM ice flows have changed to radial flows affected by local glaciers following deglaciation during Holocene time.

The sampling area of this study, the eastern basin of the Ross Sea, has a bathymetry characterized by two north trending troughs, separated by ridges. These geomorphic features were at LGM occupied by grounded ice fed by WAIS Ice Streams [*Mosola and Anderson*, 2006; *Anderson et al*., 2014]. This study follows the nomenclature given by *Mosola and Anderson* [2006] for these easternmost troughs of the Ross Sea Embayment (5 and 6, respectively). Other offshore sampling areas are located close to the coast of Marie Byrd Land, in the glacially eroded Colbeck Trough fronting Edward VII Peninsula, and in the western Sulzberger Bay, in the region east of Cape Colbeck (Figure 2).

2.2. Provenance Studies in Eastern Ross Sea and Bedrock Geochronology and Thermochronology of MBL

Paleodrainage reconstruction of LGM ice sheets was first proposed by *Hughes* [1973] based on the presence of large bathymetric troughs on the Ross Sea floor. Later, *Anderson et al*. [1983, 1992] used heavy minerals and clays from tills to reconstruct paleo ice flows on the continental shelf. Petrographic coarse sand data from *Anderson et al*. [1992] revealed an Eastern Ross Sea detrital composition made up mainly by metamorphic and felsic granitoid lithic grains. More recently, provenance studies on a till sand fraction by means of petrographic (point counting), isotopic (Sm-Nd; Pb-Pb) and geochronological (U-Pb; Ar-Ar) techniques were carried out by *Licht et al*. [2005, 2014], *Farmer et al*. [2006], and *Licht and Palmer* [2013]. The combined results of these studies demonstrated that the Ross Sea has a contribution of drainage both from EAIS and WAIS, with the convergence of the two ice flows into the Ross Sea at about 180° longitude [*Licht et al*., 2005, 2014; *Anderson et al*., 2014]. In particular *Licht et al*. [2014] provide detrital zircon U-Pb (Zrn-UPb) data from the Ross Sea and from some of the Ice Streams draining the West Antarctica Ice Sheet. Their data show an abundance of Neoproterozoic and older dates for both the Ross Sea and the Ice Stream samples. Minor populations with Cenozoic and Upper Triassic-Jurassic ages are also present. Close to our study area, *Siddoway et al*. [2004b] provide Cretaceous Zrn-UPb ages for dredged mylonites from Colbeck Trough, interpreted to be derived from Byrd Coast Granite in Edward VII Peninsula. The same authors found also Late Cretaceous AFT ages for the same samples.

Taking in consideration previous provenance studies carried out in the region, this study focus on marine piston cores distributed spatially in four main groups across Eastern Ross Sea, facing the coastal area of western Marie Byrd Land and Roosevelt Island: the easternmost group comprises three cores located close to the coast in Sulzberger Bay; the second group comprises one core in Colbeck Trough, the third group comprises six cores located in the bathymetric trough number 6 of *Mosola and Anderson* [2006]; the fourth group comprises eight cores located in trough number 5 of *Mosola and Anderson* [2006] (Figure 2).

Considering this geographical setting and sampling sites distribution, an overview of previous geochronological and thermochronological studies carried out on bedrock geology of the area is necessary. Making use of available exposures (Figure 2), several works define formation, metamorphism, and exhumation timing of the Marie Byrd Land outcropping rocks [*Pankhurst et al*., 1998; *Mukasa and Dalziel*, 2000; *Siddoway and Fanning*, 2009; *Korhonen et al*., 2010a]. Knowledge of the geological history of potential source rocks is key to detrital geochronology and thermochronology. Diagnostic criteria for age of origin of offshore sediments, gleaned from these studies, are here summarized as follows (from E to W).

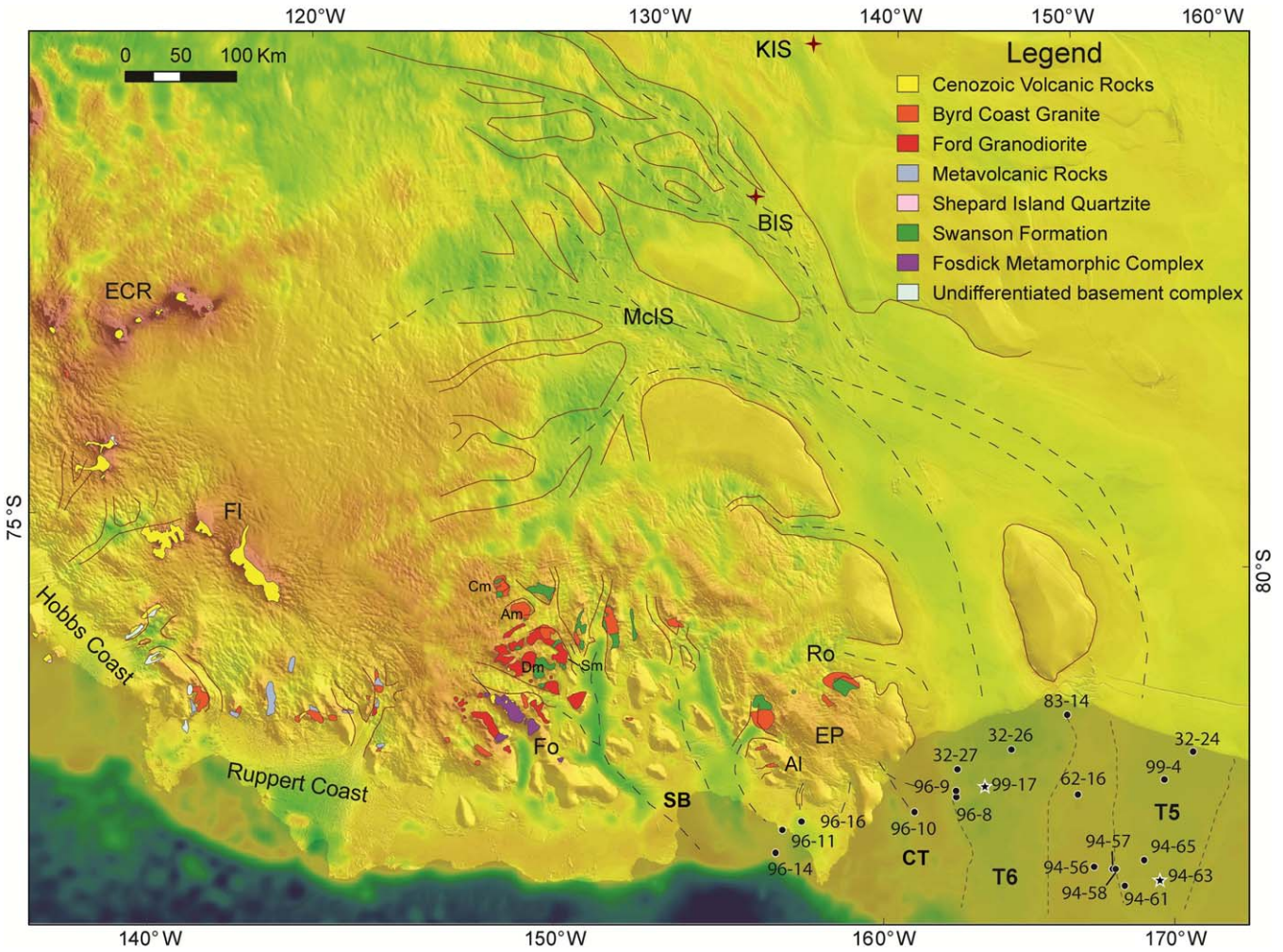

Figure 2. Bedmap geology of Marie Byrd Land, with sample locations in Eastern Ross Sea. Offshore cores labeled with a black star were studied also by *Licht et al.* [2014] as well as onshore red cross samples from Ice Streams. SB: Sulzberger Bay; Ct: Colbeck Trough; Ro: Rockfeller Mts; Al: Alexandra Mts; EP: Edward VII Peninsula; Fo: Fosdick Mts; Fl: Flood Range; ECR: Executive Committee Range; Dm: Denfield Mts; Sm: Sarnoff Mts; Am: Allegheny Mts; Cm: Clark Mts; McIS: MacAyeal Ice Stream; BIS: Bindschadler Ice Stream; KIS: Kamb Ice Stream. T5 and T6 are troughs 5 and 6 of *Mosola and Anderson* [2006], contoured by short-dashed lines. Long-dashed lines trace hypothetical flow lines. Geologic map from *Wade et al.* [1977a, 1977b, 1977c, 1978].

Mukasa and Dalziel [2000] provide Late Paleozoic and mainly Cretaceous Zrn-UPb ages in granitoids from Ruppert and Hobbs Coast. *Hart et al.* [1997] infer K-Ar ages for volcanic rocks in the Hobbs Coast ranging between 12 and 2 Ma.

On the basis of geochronological Zrn data, *Pankhurst et al.* [1998] divided Marie Byrd Land in two provinces, the westernmost one being characterized by Cambrian and Devonian-Carboniferous ages.

Yakymchuk et al. [2015] uncover detrital UPb ages of the sedimentary Swanson Fm., in the Ford Ranges, with a major Neoproterozoic-Cambrian (500–750 Ma) and minor Mesoproterozioc (930–1180 Ma), Paleoproterozoic (1560–1930 Ma), and Paleozoic (387 $\pm$ 22 Ma) age populations.

Zrn-UPb ages of the Fosdick Mountains migmatite-granite complex [*Siddoway and Fanning*, 2009; *Brown et al.*, 2016] define intervals of 370–355 Ma and 118–90 [*McFadden et al.*, 2010a, 2010b; *Brown et al.*, 2016] for plutonism and migmatization.

McFadden et al. [2010a, 2010b], *Saito et al.* [2013], and *Brown et al.* [2016] present UPb ages for zircons and titanite in the Fosdick Mountains plutons, mafic dykes and migmatites, yielding Cretaceous crystallization ages (Byrd Coast Granite age). *Richard et al.* [1994] provide AFT, Ar/Ar, and Monazite UPb data for high-grade metamorphic rocks in the Ford Ranges, yielding Cretaceous to Eocene ages.

Contreras et al. [2012] present zircon UPb and U-Th/He dates on metasedimentary gneisses and granites between Alexandra (Edward VII Peninsula) and Fosdick Mountains (Ford Ranges), yielding major detrital populations of 1000–1100 and 500 Ma, and Middle-Late Cretaceous crystallization-cooling ages.

Adams et al. [1995] carried out a geothermochronometric study of the Edward VII Peninsula (Alexandra and Rockfeller Mountains), revealing regional metamorphism at 421–432 Ma (Rb-Sr dates of the Swanson Formation), emplacement of granites and thermal metamorphism in the Cretaceous (95–105 Ma, K-Ar dates of granites). Upper Cretaceous-Paleocene (98–55 Ma) zircon fission track and AFT data from this work and *Siddoway et al*. [2004b] indicate the period of regional cooling and uplift started concurrently to granite emplacement.

Lisker and Olesch [1998] infer from AFT data three distinct periods of cooling for the Edward VII Peninsula and the Ford Ranges (100–85; 70–65 and since the Oligocene), attributed to a pulsing mantle plume. *Spiegel et al*. [2016] provide zircon fission track data (108–80 Ma), AFT (93–28 Ma), and apatite (U-Th)/He (128–5 Ma) data for the Hobbs Coast and eastern Marie Byrd Land.

As a whole these data describe a Precambrian-Cambrian basement, undergoing several episodes of magma intrusion, metamorphism, migmatization, and regional uplift and cooling (Devonian-Carboniferous; Cretaceous-Paleocene), and a major volcanic and localized uplift-cooling stage since the Oligocene. From such a bedrock picture single grain detrital samples are expected to be mainly Neoproterozoic, Devonian-Carboniferous, Triassic-Jurassic, or Cretaceous for the Zrn-UPb, and mainly Late Cretaceous-Cenozoic for the AFT.

3. Materials, Methods, and Results

3.1. Sampling Strategy

A total of 19 LGM and post-LGM piston cores collected by different scientific cruises across the Eastern Ross Sea was logged and sampled at the Marine Geology Antarctic Research Facility of Tallahassee, Florida. Distribution map and list of samples are shown in Figure 2 and Table 1. The rationale of the choice of these piston cores is based on their geographic distribution, sediment recovery, and presence of clast-rich glacial till sedimentary facies. Figure 2 shows geographic location of sites, which are distributed over the Eastern Ross Sea and can be grouped in four different subareas: Sulzberger Bay on the east, Colbeck Trough close to the coast of Edward VII Peninsula, trough 6 in the central subarea and trough 5 on the west of the study area (following the nomenclature applied by *Mosola and Anderson* [2006], Figure 2).

Table 1. List of Sample Sites From Eastern Ross Sea and Analytical Techniques Carried Out[a]

Area	Cruise	Core	Label	Latitude	Longitude	Water Depth(m)	Core Length(cm)	Clast Log	N° Clasts	Sampled Clasts	UPb	AFT
Sulz.Bay	NBP96-01	011-PC	96-11	−76.78	−155.44	392	389	x	259	9		x (40–43)
Sulz.Bay	NBP96-01	014-PC	96-14	−76.59	−155.55	369	154	x	48	5		
Sulz.Bay	NBP96-01	016-PC	96-16	−76.91	−155.93	1273	65	x	172	2		x (2–6)
Colbeck Trough	NBP96-01	010-PC	96-10	−77.23	−160.11	493	190	x	13	1	x (188–190)	x (9–14; 25–29; 188–190)
T6	NBP96-01	008-PC	96-08	−77.56	−160.94	650	202	x	163	12		
T6	NBP96-01	009-PC	96-09	−77.61	−160.85	643	210	x	58	8		
T6	ELT32	027-PC	32-27	−77.78	−160.63	670	148	x	185	14		x (55–60; 105–110)
T6	NBP99-02	017-PC	99-17	−77.72	−161.86	715	205	x	33	14		x (134–139)
T6	ELT32	026-PC	32-26	−78.07	−162.39	605	247	x	29	13		
T6	DF83	014-PC	83-14	−78.48	−164.14	601	277	x	40	14	x (231–236)	x (81–86; 183–190; 231–236)
T6/T5	DF62-01	016-PC	62-16	−77.97	−165.83	467	229					x (111–117; 151–156)
T6/T5	NBP94-07	056-PC	94-56	−77.33	−166.66	441	362	x	60	15		
T5	ELT32	024-PC	32-24	−78.40	−169.13	565	433				x (142–146)	x (416–420)
T5	NBP94-07	057-PC	94-57	−77.34	−167.36	525	89	x	23	4		
T5	NBP94-07	058-PC	94-58	−77.35	−167.46	525	315	x	53	8		x (170–173)
T5	NBP94-07	061-PC	94-61	−77.23	−168.04	548	36	x	8	1		
T5	NBP94-07	063-PC	94-63	−77.33	−169.18	582	292	x	53	9		
T5	NBP94-07	065-PC	94-65	−77.47	−168.44	587	116	x	13	8		
T5	NBP99-02	004-PC	99-4	−78.15	−168.58	618	104	x	18	8		

[a]The same sites are shown labeled in Figure 2 and elsewhere in the text. Clast log includes gravel-size clasts identification, classification, and sampling of selected clasts for detailed petrographic analysis. Also the sampling depths in cm for Upb and AFT analysis are shown. Abbreviations: Sulz.Bay: Sulzberger Bay; T5 and T6: trough 5 and trough 6 from *Mosola and Anderson* [2006].

Logging was aimed to identify the distribution and the features of the gravel fraction (i.e., granule to cobble size clasts) along the entire length of each core. The size, shape and features of each clast >2 mm was determined for each 10 cm interval of the working half split surface of the core. On the basis of distinctive macroscopic features, clasts were grouped into six major lithological groups (volcanic rocks; intrusive rocks; metamorphic rocks; sedimentary rocks; quartz; dolerite). Data acquisition also involved subdivision and counting of clasts occurrence in each group for each 10 cm interval of the cores. A summation of all clasts from different lithological groups was carried out for each core. Table 1 shows also number of logged clasts for each half split surface of cores. A total amount of 1118 clasts were counted and measured from the 19 cores and from these 210 representative clasts (granule to cobble size) were sampled for petrographic analysis. Furthermore, 15 bulk till sand-rich intervals (2–5 cm thick) were sampled for geochronological and thermochronological analysis on the granulometric fraction comprised between 63 μm and 2 mm. Sampling depths for geochronological and thermochronological analysis are listed in Table 1.

3.2. Petrography

3.2.1. Analytical Details

A selection of 51 representative pebble sized clast thin sections was examined under a polarizer microscope in order to establish a detailed mineralogical and textural analysis for each sample. The identification of possible source rocks for pebbles was carried out thanks to a representative collection of Marie Byrd Land rocks stored at the Polar Rock Repository at the Byrd Polar and Climate Research Center (Ohio State University).

3.2.2. Petrographic Results

On the basis of detailed petrographic analysis, clasts recovered from the piston cores can be grouped in the following four main lithological groups (Table 2 and Figure 3):

1. Igneous plutonic rocks, including undeformed biotite-hornblende granodiorite and tonalite, biotite monzogranite, alkaline feldspar quartz-syenite, leucocratic biotite syeno-granite (334 total clasts).
2. Igneous subvolcanic and minor volcanic rocks, including syeno-granite, monzonitic and mafic porphyries, dolerites, trachyte, and rare felsic volcanics (25 total clasts).
3. Low-grade metamorphic rocks, including biotite hornfels, biotite $\pm$ white mica schists, biotite-actinolite schists, quartzites, metasiltstones, metasandstones, phyllites, slates (604 total clasts).
4. Sedimentary rocks, including lithic graywackes, impure quartz-arenites, siltstones, and mudstones (85 total clasts).

Two main types of granitoids were distinguished among the samples: black and white biotite $\pm$ hornblende monzogranite, granodiorite, and tonalite (type A in Table 2 and Figure 3) are slightly foliated inequigranular, medium to coarse grained, with hypidiomorphic texture. Biotite is sometimes replaced by chlorite, while feldspars present a light to strong alteration in sericite; quartz is anhedral and interstitial to euhedral plagioclase. Accessory phases are titanite, apatite, zircons, allanite, and opaque minerals. The second variety is composed by slightly foliated pinkish, inequigranular to slightly equigranular, medium to coarse grained, porphyritic biotite monzogranite and leuco syeno-granites (type B in Table 2 and Figure 3), with hypidiomorphic texture. Ortoclase is perthitic and slightly altered in sericite. Accessory phases comprise apatite, zircon/monazite, and opaque minerals.

Light gray syeno-granite porphyry (Thin section 14) consists of inequigranular porphyritic texture, with mm sized euhedral phenocrysts of K-feldspar, subrounded quartz, and plagioclase set in a fine-grained quartz and feldspar groundmass. Dolerite (Thin section 17) has inequigranular fine to medium grained subophitic texture, with small plagioclase laths intergrowth with larger clinopyroxene crystals and small altered olivine crystals. In another Thin section (23), dolerite has a slightly spherulitic texture, with crystals of plagioclase and clinopyroxene set in a matrix of opaque minerals. Mafic rocks include doleritic porphyries, characterized by holocrystalline fine to medium grained porphyritic textures, with phenonocrysts of plagioclase and clinopyroxene set in a microcrystalline plagioclase-clinopyroxene-opaque minerals groundmass. In one case (i.e., Thin section 16), clinopyroxenes appear to be completely altered.

Among volcanic rocks, one sample (60) of dark gray trachyte was found: it has a finely porphyritic holocrystalline trachytic texture with oriented microliths of K-feldspar set in a groundmass of opaque minerals and altered clinopyroxene. Other samples of volcanic rocks are a basaltic vescicular scoria (Thin section 69), a very altered olivine basalt (Thin section 66) with aphanitic hypocrystalline texture, and a rhyolitic volcanic rock with flow texture and phenonocrysts of embayed quartz and alkaline-feldspar (Thin section 68).

Table 2. Petrographic Characteristics of Sampled Gravel-Sized Clasts Recovered From Eastern Ross Sea Piston-Cores[a]

Thin Section	Cruise	Core	Top	Bottom	Lithology	Pl (%)	Cam (%)	Bt (%)	Qtz (%)	Opm (%)	Kfs (%)	Cal (%)	Cpx (%)	Ol (%)	Grt (%)	Czo-Ep (%)	Ttn (%)	Ap (%)	Zrn (%)	Chl (%)	Wm (%)	Lithics (%)	Matrix (%)	Groundmass (%)	Glass (%)	Grain Size
1	NBP96-01	11-PC	261	262	Bt-granodiorite/tonalite	40		10	40	<1	10							<1	<1	<1						mg
2	NBP96-01	11-PC	291	292	Bt-granodiorite	38		4	41	<1	16					<1		<1	<1	<1	<1					fg-mg
3	NBP96-01	11-PC	295	297	Bt-cam-schist	32	8	21	36	<1						<1		<1		2						fg-mg
4	NBP96-01	11-PC	310	312	Bt-monzogranite	27		10	30		32					<1		<1	<1		<1					mg-cg
5	NBP96-01	14-PC	43	44	Alcaline feldspar quartz-sienite	5		7	18	<1	69							<1	<1	<1						mg-cg
6	NBP96-01	14-PC	84	85	Sub-litharenite	2			78	3		9				<1				<1	1	6				mg
7	NBP96-01	16-PC	62	65	Bt-bearing leucocratic syeno-granite	18		1	22	1	57							<1		<1	<1					mg
8	NBP96-01	16-PC	62	65	Graywacke	3			81	1		5							<1	3	1	5				mg
9	ELT32	27-PC	117	118	Bt-pl schist	25		8	65	<1								<1	<1							fg
10	NBP96-01	08-PC	99	100	(meta) Sandstone	1			79	1		15								<1	3					fg
11	NBP96-01	08-PC	111	112	Meta sandstone (hornfels)	1		6	70			4								12	7					mg
12	NBP99-02	17-PC	16	19	Cataclasite				35			49				<1				2				13		fg-mg
13	NBP99-02	17-PC	1	3	Bt-tonalite	40		8	42	1	8							<1	<1	<1						mg
14	DF83	14-PC	23	25	Leucocratic syeno-granite porphyry	15		<1	40		45								<1	<1	<1					mg-cg
15	DF83	14-PC	241	245	Bt-Hbl-tonalite	57	15	2	20	1	5						<1		<1	<1						mg
16	DF83	14-PC	252	256	Meta-pl-cpx-porphyry	45			8	3		2	4			1				5				31		mg
17	NBP 94-07	057-PC	15	16	Dolerite	48				1			35	4						12						mg
18	NBP 94-07	057-PC	36	37	Bt-Hbl-tonalite	63	7	5	18	1	2						<1	<1	<1	3						mg
19	NBP 94-07	058-PC	113	117	Meta-vulcano-clastite	4			15	1		23				12				12		21		12		mg-cg
20	NBP 94-07	063-PC	213	214	Bt-Act-schist	12	4	28	49			3						<1		2	1					fg-mg
21	NBP99-02	04-PC	8	9	Bt-Wm-gneissic schist	21		12	61	1								<1			5					mg
22	NBP99-02	04-PC	34	35	Wm-opm rich-metasandstone				68	15						3				2	12					vfg-mg
23	NBP99-02	04-PC	92	93	Dolerite	45			2	1			34			3				15						fg-mg
42	ELT32	27-PC	49	52	Qtz arenite	3			80			1								5	1	1	9			fg-mg
43	ELT32	27-PC	68	72	Meta-siltstone																					fg
44	ELT32	27-PC	135	138	Medium grained graywacke	2			76			18									2	2	12			mg
45	NBP99-02	17-PC	77	82	Qtz-arenite				93	1		1								<1	2	3				mg-cg
46	NBP99-02	17-PC	176	180	Impure arenite/graywacke				46	3		50										1	50			fg-mg
47	ELT32	26-PC	140	146	Bt-gneiss	34		12	51	1								<1			1					mg
48	ELT32	26-PC	237	238	Siltstone																					vfg-fg
49	DF83	14-PC	208	210	Meta-siltstone																					fg
50	DF83	14-PC	31	33	Coarse grained sub-litharenite				88	2		3									1	5	7			mg-cg
51	DF83	14-PC	269	273	Medium grained qtz-arenite				98	1											1	<1	<1			mg
52	NBP 94-07	058-PC	55	57	Slate																					vfg
53	NBP 94-07	058-PC	121	125	Quartzite	1			89	1										7	2					fg-mg
54	NBP 94-07	063-PC	222	223	Hbl-gneiss	2	7	4	72	2		4			2		<1	<1		4	2					mg-cg
55	NBP 94-07	063-PC	11	14	Meta-vulcano-clastite	4	12		53	1										30						mg
56	NBP 94-07	056-PC	140	142	Wm-metasandstone	2			80	4											8					fg-mg
57	NPP 94-07	056-PC	216	217	Qtz-arenite	<1			95	1	1	<1										<1				mg
58	NBP 94-07	056-PC	234	235	Siltstone																					vfg
59	NBP 94-07	056-PC	305	308	Bt-Hbl-tonalite	59	5	4	24	1	5						1	<1	<1							mg-cg
60	NBP 94-07	065-PC	31	34	Trachyte	10				14	63		12	1												fg
61	NBP 94-07	065-PC	16	18	Qtz-siltstone					3		1									1					vfg
62	NBP96-01	09-PC	5	6	Bt-Wm-granofels	11		37	46	1								<1			5					mg
63	NBP96-01	09-PC	122	124	Calc-schist	2			53	1		35									9					fg
64	NBP96-01	09-PC	145	150	Medium grained (meta)arenite	2			81	1		10									4	1				fg-mg
65	NBP 94-07	058-PC	225	226	Mafic porphyry (altered)	15			8(s)			45(s)												32		
66	DF83	14-PC	90	94	Olivine basalt (altered)	25				10			2	7											56	vfg
67	ELT32	27-PC	34	36	Cpx-porphyry	10							35							5(s)	2(s)			47		fg-mg
68	NBP 94-07	065-PC	17	20	Felsic volcanic	5			22		12						<1							61		mg
69	NBP 94-07	063-PC	227	228	Basaltic scoria	2								1											97	

[a]Also geographic areas referring to piston cores location and labels of sampling sites, as shown elsewhere in the text and in Figures 2 and 7, are listed. Mineral abbreviations according to *Kretz* [1983] except for Wm: white mica and Opm: opaque minerals. Petro type—IP: igneous plutonic; S: sedimentary; M: metamorphic; IV: igneous volcanic; ISv: igneous subvolcanic. Grain size—Cg: coarse grained; mg: medium grained; fg: fine grained; vgf: very fine grained. Top and bottom refer to sampling depth along the cores, expressed in centimeters. T5 and T6 are trough 5 and trough 6 from *Mosola and Anderson* [2006].

AGU Geochemistry, Geophysics, Geosystems

10.1002/2016GC006728

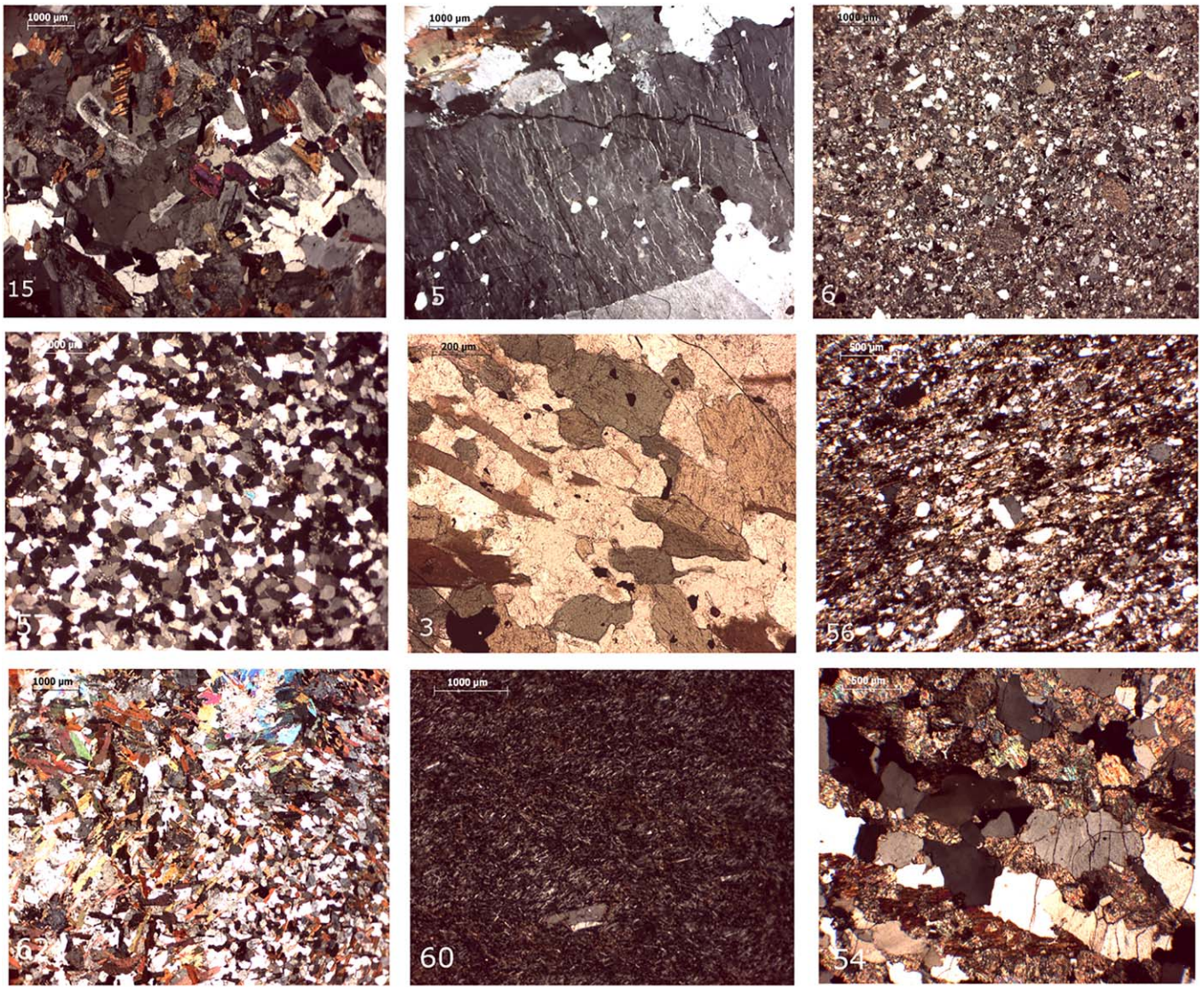

Figure 3. Photomicrographs of representative clasts recovered in Eastern Ross Sea cores: Thin section 15 (core 83–14, crossed polarizers): bt-hbl tonalite showing medium grained hypidiomorphic texture (type A granitoid); Thin section 5 (core 96–14, crossed polarizers): coarse grained alkali feldspar quartz-syenite (type B granitoid); Thin section 6 (core 96–14, crossed polarizers): fine to medium grained heterogranular sublitharenite; Thin section 57 (core 94–56, crossed polarizers): medium grained qtz-arenite; Thin section 3 (core 96–11, planed polarizers): bt-hbl schist with foliation defined by orientation of mica and amphibole; Thin section 56 (core 94–56, crossed polarizers): white mica metasandstone; Thin section 62 (core 96–9, crossed polarizers): biotite-white mica hornfels; Thin section 60 (core 94–65, crossed polarizers): trachyte with holocrystalline oriented fine-grained texture; Thin section 54 (core 94–63, crossed polarizers): biotite-hornblende gneiss.

The group of low-grade metamorphic rocks comprises metasiltstones, metasandstones, phyllites, slates, quartzite, biotite hornfels, biotite ± amphibole schists, and rare gneisses. Metasandstones are fine to medium grained, with well-preserved bedding and clastic texture. Grains are composed mainly of quartz, with minor amount of feldspars, which are set in recrystallized matrix composed of chlorite, muscovite and calcite, and sometimes oxides. Phyllites display of a very weak fine-grained foliation defined by orientation of white mica, chlorite, and rare biotite flakes, set in a mainly quartzose and carbonate equigranular matrix. Slate is characterized by a well-defined quartz and opaque minerals cleavage, with a spotted texture formed by Fe-oxides porphyroblasts (Thin section 52). Hornfels are mainly of sedimentary origin: they preserve clastic texture, with fine to medium grained granoblastic quartz domains and randomly oriented biotite and chlorite flakes, which sometimes form spotted structures. Biotite schists show fine to medium grained grano-lepidoblastic texture, with foliation defined by orientation of biotite and poikiloblastic actinolite, and granoblastic domain defined by interlobate quartz and plagioclase aggregates (Thin section 20). In some cases, amphibole is absent and the foliation is defined by biotite and rare white mica (Thin section 21).

One sample (Thin section 54) is characterized by gneissic layering defined by granoblastic interlobate quartz and plagioclase domains associated with nematoblastic hornblende and rare garnet.

Sedimentary rocks are mainly siltstones, graywackes, and medium grained quartz-arenite. Dark gray to black siltstones are composed of very fine-grained quartz grains set in a matrix of clay and opaque minerals. Graywackes consist of fine to medium grained sands composed by quartz and minor amount of feldspars. Low-grade metamorphic and siliceous lithic fragments are prevalent, set in a matrix of clay, calcite, and sometimes chlorite. Brown to pinkish quartz-arenites are heterogranular, medium to coarse grained, with prevalent subrounded quartz grains and minor amount of feldspars, chert and low-grade metamorphic lithic fragments. The cement consists sometimes of authigenic quartz overgrowth and sometimes of carbonates.

3.2.3. Clasts Distribution

The Sulzberger Bay cores are characterized by a distinct clast assemblage, with core 96–14 dominated by low-grade metamorphic rocks (81%), followed by granitoids and subordinate sedimentary rocks; on the other side, core 96–11 shows a prevalent granitoid lithology of clasts (79%) and a minor metamorphic component. Core 96–16 has a mixed composition with prevalent granitoids (40%), with subordinate metamorphic (27%) and sedimentary clasts (17%). Considering all the counted clasts together as a single group, these three cores have an overall composition consisting of dominant granitoids rock fragments (66%), and minor low-grade metamorphic rocks (15%), quartz (10%), and sedimentary rocks (9%).

Trough 6 cores have an overall clasts distribution more homogeneous than the Sulzberger Bay group (Figures 2 and 7). In every core, the predominant lithology among the counted clasts is low-grade metamorphic rock, followed in general by sedimentary clasts and granitoids; only in one case (core 83–14) do granitoids prevail over sedimentary rock fragments in counted clasts. Volcanic and subvolcanic clasts are rare and occur only in the westward three cores, distributed from the center of the trough to its border, close to the Ice Shelf margin. The minor amount of granitoid clasts is reflected also in the overall composition of this group, with 75% clasts composed of low-grade metamorphic rock fragments, 12% of sedimentary rock fragments, and 5% of granitoids, with minor amount of volcanic and subvolcanic clasts.

Also in the case of trough number 5 of *Mosola and Anderson* [2006] (Figures 2 and 7), low-grade metamorphic rocks are the most widespread lithologies among the counted clasts in the cores, with a percentage range of 50 and 72%. Granitoids are the second most represented lithology in all but one of the cores (99–04), followed by sedimentary clasts and minor mafic porphyries, dolerites, and volcanic rocks. In this trough, granitoids are more abundant than sedimentary clasts, ranging from 50% in 94–61 core to 6% in 99–04 core. Volcanic rocks are minor, but are present in four out of eight cores, with a peak occurrence in core 99–04 with 17% of the total. Subvolcanic mafic porphyries and dolerites are present in minor amount in five out of eight cores, with the maximum occurrence of 8% in 94–65 PC. Counting all the clasts together as a single group, the trough 5 cores have an overall clast assemblage including 64% of metamorphic clasts, 24% of granitoids, 4% of sedimentary clasts, and minor amounts of subvolcanic and volcanic rocks.

3.3. Mineral Chemistry

3.3.1. Analytical Details

Mineral chemistry analyses were carried out on 10 representative clasts. They were chosen on the basis of the presence of minerals such as amphiboles and white micas and considering also their lack of alteration. Only samples with fresh mineral surfaces were chosen. They include biotite amphibole schist (Thin sections 3 and 20), fine to medium grained metasandstones (Thin sections 11 and 56), biotite-hornblende tonalite (Thin section 59), biotite-white mica gneissic schist (Thin section 21), biotite gneiss (Thin section 47), biotite-hornblende gneiss (Thin section 54), biotite-white mica hornfels (Thin section 62), and fine-grained calc-schist (Thin section 63). Chemical analysis of the main mineral phases identified via petrographic microscope were carried out with an X-ray energy dispersive system EDAX DX4 attached to a Scansion Electron Microscope Philips XL30 at the Department of Physical Sciences, Earth and Environment of Siena (Italy). Selected thin sections have been polished and carbon coated before carrying out measurements. Analytical conditions were 20 kV of accelerating voltage, 25 μA of emission current, and a beam spot size of 0.2 Am. Natural minerals were used as standards. Fe^{3+} concentration in clinoamphiboles and clinopyroxenes was estimated by the equation of *Droop* [1987], assuming charge balance.

3.3.2. Mineral Chemistry Results

Chemical analysis of bulk-rock samples from western Marie Byrd Land are available in literature [*Weaver et al*., 1991, 1992; *Korhonen et al*., 2010b; *Yakymchuk et al*., 2015; *Brown et al*., 2016]. However, published mineral chemistry analyses from the region are sparse. One example is *Smith* [1996] in which mineral data of migmatitic paragneiss from Scott Nunataks (Alexandra Mountains) are presented.

In this work, also minerals from one sample of biotite-hornblende Ford granodiorite from Lewis Rocks (Phillips Mountains) and one sample of Swanson Formation phyllite from Bailey Ridge (Sarnoff Range), both stored at the Polar Rock Repository at the Byrd Polar and Climate Research Center (Ohio State University), were analyzed. The latter were chosen because they showed similar petrographic features with some of the detrital clasts recovered offshore and to better check the possibility of a comparison with some bedrock sources.

Clinoamphiboles, biotites, and white micas composition are shown in Figure 4. All analyzed amphiboles are members of the calcic-amphibole group (Figure 4a) [*Leake et al*., 1997]. Clinoamphiboles in biotite-amphibole schist (Thin section 20) are actinolitic hornblendes to actinolites in composition, with X_{Mg} varying from 0.63 to 0.80, and they are slightly zoned, with a Fe-richer core and a Mg-richer rim. In gneiss (Thin section 54), amphiboles are mostly Mg-hornblendes to actinolitic hornblendes (X_{Mg} ranging from 0.67 to 0.82), having a weak zonation, with Fe-richer rim and Mg-richer core in most cases. In tonalite (Thin section 59) amphiboles are mainly Mg-hornblendes (X_{Mg} 0.68–0.76), in some cases zoned, with a Mg-richer core

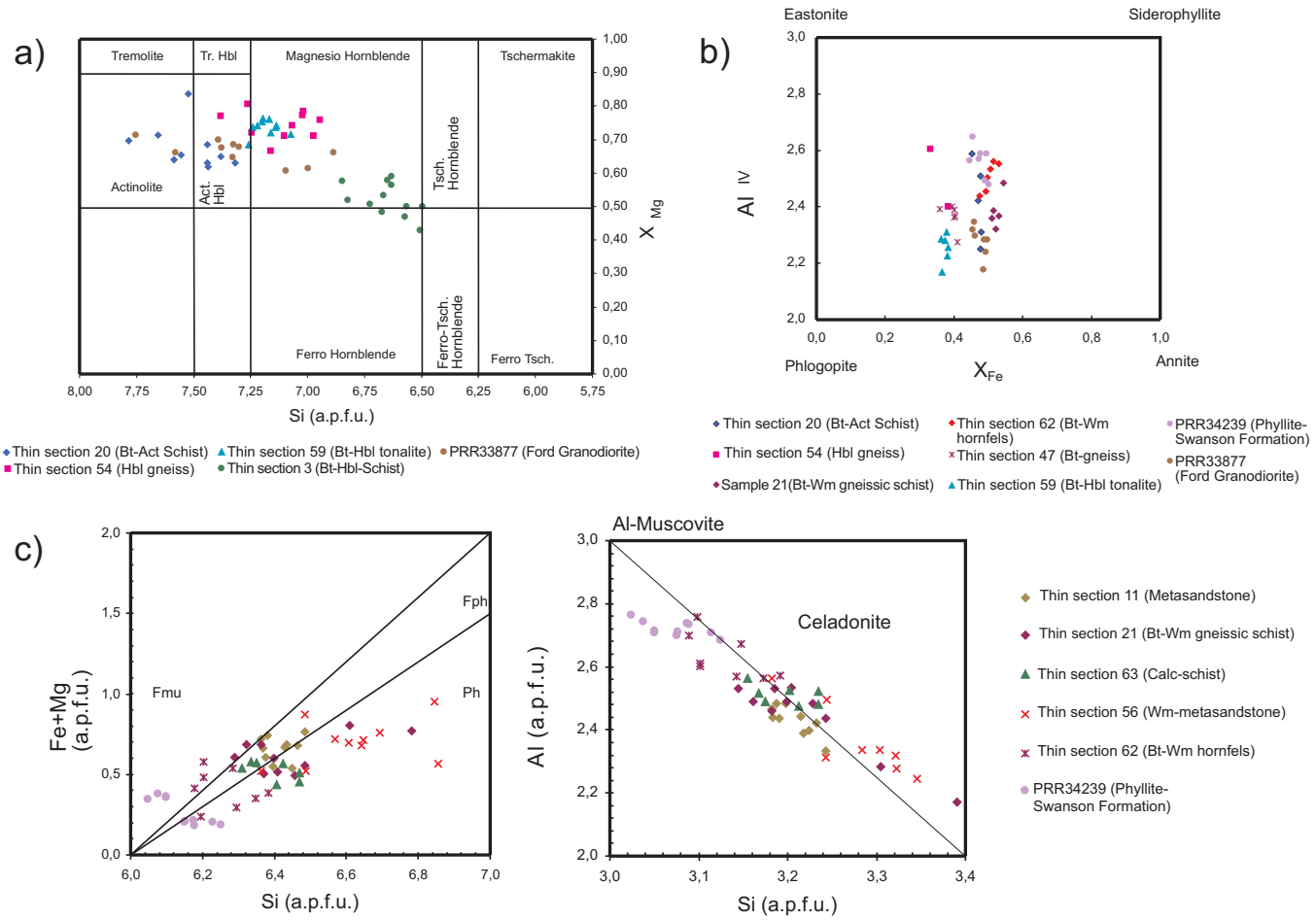

Figure 4. Representative chemical analysis of minerals from Eastern Ross Sea detrital clasts: (a) Ca-amphibole classification from *Leake et al*. [1997], in terms of X_{mg} versus Si (atoms per formula unit); (b) biotite composition in terms of Al^{IV} versus Fe/(Fe + Mg); (c) white mica composition in terms of Fe + Mg versus SI and Al versus Si (atoms per formula unit). PRR33877 and PRR34239 are samples from bedrock, respectively from Ford Granodiorite and Swanson Formation, stored at the Polar Rock Repository, Ohio State University. Mineral abbreviation from *Kretz* [1983] except for Wm = white micas.

and a Fe-enriched rim. In biotite schist (Thin section 3), amphiboles are distributed around the boundary between Mg-hornblende and Fe-hornblende fields (X_{Mg} 0.43–0.59).

Biotite representative compositions are listed in Figure 4b. In some samples (e.g., Thin section 62), biotites have a wide compositional range (X_{Fe} from 0.45 to 0.55) and exhibit a strong zonation, with Fe enrichment and Mg depletion from core to rim. In tonalite (Thin section 59), biotites show the lowest X_{Fe} values (0.37–0.39). Biotite-white mica schist (Thin section 21) and biotite-amphibole schist (Thin section 20) show a compositional range, with X_{Fe} ranging from 0.50 to 0.55 and 0.45 to 0.48, respectively.

White mica representative compositions are listed in Figure 4c. White micas in metasandstone (Thin section 11), calc-schist (Thin section 63), biotite-white mica hornfels (Thin section 62), and gneissic schist (Thin section 21) are all muscovite, with a wider and more phengitic composition in the latter. White micas in the other analyzed metasandstone (Thin section 56) show a wide and prevalently phengitic composition, with Si (a.p.f.u.) ranging from 6.36 to 6.86.

3.4. Zircon U-Pb Geochronology

3.4.1. Analytical Details

Zircon U-Pb dating was performed on three piston core samples (96–10; 83–14; 94–63, sampling depths are listed in Table 1) at the LA-ICP-MS lab at the Consiglio Nazionale della Ricerche (CNR)-Istituto di Geoscienze e Georisorse Unità di Pavia (Italy), following the analytical conditions described in *Langone et al*. [2014]. Samples were taken from sand-rich intervals in order to obtain as much datable grains as possible; the choice of cores was determined by their geographic location, which cover an extensive area from Colbeck Trough (core 96–10) close to Cape Colbeck in Edward VII Peninsula to trough 6 close to the coast of Roosevelt Island (core 83–14) and trough 5 (core 94–63). Sampling site locations are shown in Figure 2.

Zircon grains were separated from 100 cm^3 bulk samples after careful crushing using heavy liquids and magnetic separation techniques. Zircon grains were then mounted in 1 in. epoxy-filled mount, and polished to obtain even surfaces suitable for cathodoluminescence (CL) imaging and LA-ICP-MS analyses. Prior to age determination, the internal structure of the zircons was investigated with backscattered electron (BSE) microscopy and CL using a Philips XL30 electron microscope equipped with a Centaurus CL detector. Prior to the CL imaging, the samples were carbon coated and the images were obtained using 15 kV acceleration voltage and a working distance of 26 mm. Age determinations were performed using a 193 nm ArF excimer laser microprobe (GeoLas200QMicrolas) coupled to a magnetic sector ICP-MS (Element 1 from ThermoFinnigan). Analyses were carried out in single spot mode and with a spot size fixed at 25 μm. The laser was operated with a frequency of 5 Hz, and with a fluence of 8 J/cm^2. Sixty seconds of background signal and at least 30 s of ablation signal were acquired. The signals of masses ^{202}Hg, $^{204}(PbHg)$, ^{206}Pb, ^{207}Pb, ^{208}Pb, ^{232}Th, and ^{238}U were acquired in magnetic scan mode. ^{235}U is calculated from ^{238}U based on the mean ratio $^{238}U/^{235}U$ of 137.818, as recently proposed by *Hiess et al*. [2012]. The 202 and 204 masses were collected in order to monitor the presence of common Pb in zircon (more analytical details in *Tiepolo* [2003] and *Paquette and Tiepolo* [2007]), with the signal of ^{202}Hg acquired to correct the isobaric interference of ^{204}Hg on ^{204}Pb [*Horn et al*., 2000]. Mass bias and laser-induced fractionation were corrected by adopting external standards, the GJ-1 zircon standard (608.5 ± 0.4 Ma) [*Jackson et al*., 2004]. During an analytical run of zircon analyses, a reference zircon (02123, 295 Ma) [*Ketchum et al*., 2001] was analyzed together with unknowns for quality control. Data reduction was carried out through the GLITTER software package [*Van Achterbergh et al*., 2001]. Time-resolved signals were carefully inspected to detect perturbation of the signal related to inclusions, cracks, or mixed-age domains. Within the same analytical run, the error associated with the reproducibility of the external standards was propagated to each analysis of sample [see *Horstwood et al*., 2003], and after this procedure each age determination was retained as accurate within the quoted error. The Concordia test was performed for each analytical spot from $^{206}Pb/^{238}U$ and $^{207}Pb/^{235}U$ ratios using the function in the software package Isoplot/Ex 3.00 [*Ludwig*, 2003]. Percentage of discordance has been calculated as {[1($^{206}Pb/^{238}U$ age/$^{207}Pb/^{235}U$ age)] × 100}, and only the U-Pb ages with a percent of discordance $<\pm 1.5\%$ were considered reliable. Errors in the text and figures are reported as 2σ. Discordant data were not taken into consideration because of doubtful interpretation. The Isoplot software was also used to draw concordia diagrams and probability density plots. U-Pb isotope analyses and calculated ages of zircons are reported in the data repository.

3.4.2. Zircon U-Pb Geochronology Results

Zircon U-Pb results are reported in Table 3 and in Figure 5. This figure displays the data from three new samples together with the data of *Licht et al*. [2014], in geographic order from East to West.

Sample from core 96–10 is characterized by zircon with various crystal shapes, from elongated to short, rounded and abraded, with internal features, as shown by CL imaging, varying from continuous oscillatory zoning to homogenous low CL core and rims, separated by high CL bands/domains. Eighty-one analyses were carried out, and 44 concordant ages were obtained.

Sample from core 83–14 yields generally zircon grains in a good state of conservation, with shapes varying from elongated to short. CL imaging highlights different kinds of zonation, from continuous oscillatory to high CL core and rims separated by low CL bands. Ninety-two analyses were performed and 52 concordant ages were obtained.

Sample from core 32–24 shows zircon grains with variable crystal shapes, from elongated to short, and several grains appear rounded and abraded. Zonation is very variable, with some crystals showing continuous oscillatory zonation, and others showing alternating homogeneous high and low CL bands and oscillatory zonation bands. Eighty-two concordant dates were obtained from 106 analyses.

Among the three analyzed samples five age populations could be identified.

A significant Cretaceous-Paleocene (63–139 Ma) population is present in samples from cores 96–10 (Colbeck Trough) and 83–14 (Roosevelt Island), whereas it is minor in sample 32–24 (trough 5).

A Devonian-Carboniferous (311–360 Ma) population is present in samples from cores 96–10 and 83–14. This population is absent in sample from core 32–24, where a Late Triassic (201 Ma) population is instead present.

A Neoproterozoic-Cambrian (492–566 Ma) population is minor in sample from core 96–10 and major in samples from cores 83–14 and 32–24.

Subordinate Precambrian (987–1039; 1457; 2155 Ma) populations are present only in samples from cores 83–14 and 32–24.

These results resemble the data of *Licht et al*. [2014] in most respects (Figure 5).

3.5. Apatite Fission Track Thermochronology

3.5.1. Analytical Details

Apatite fission-track analysis was performed on grains acquired from nine piston core samples. The latter are, located from east to west, 96–11, 96–16, 96–10, 32–27, 99–17, 83–14, 62–16, 32–24, and 94–58. Sampling depths are listed in Table 1 and core sites are shown in Figure 2. Samples were analyzed at the Fission Track laboratory of the University of Padua. As for UPb analysis, samples were chosen from sand-rich intervals of the cores and following the widest geographic distribution across the study area. Apatite grains were separated from 100 cm^3 bulk samples after careful crushing using heavy liquids and magnetic separation techniques. Mounts of apatites in epoxy were ground and polished to expose planar surfaces within the grains and then etched with 5 N HNO_3 at 20°C for 20 s to reveal spontaneous fission tracks. Samples then were irradiated with thermal neutrons in the reactor at the Radiation Center of Oregon State University with a nominal neutron fluence of 9×10^{15} n cm^2. The CN-5 dosimeter was used to measure neutron fluence. After irradiation, induced fission tracks in the low-U muscovite that covered apatite grain mounts and glass dosimeter were revealed by etching in 40% HF at 20°C for 40 min. Apatite FT dates (up to 40 grains per sample; analyst: Dr. B. Andreucci) were calculated using the external-detector and the zeta-calibration methods [*Hurford and Green*, 1983] with IUGS age standards (Durango and Fish Canyon apatites) [*Hurford*, 1990] and a value of 0.5 for the 4p/2p geometry correction factor. The observed grain-age distributions were decomposed into different component populations by using the binomial peak-fitting method [*Brandon*, 1996]. This technique is based directly on the bimodal distribution that best represents counting statistics for FT dating. Individual fitted peaks have a mean age and standard error.

3.5.2. AFT Thermochronology Results

Apatite fission-track results are reported in Table 4 and Figure 6; 40–100 grains were dated for each of nine cores, allowing a good decomposition into different populations. Where multiple samples from a single

Geochemistry, Geophysics, Geosystems

10.1002/2016GC006728

Table 3. Isotopic Data and U-Pb Ages of Zircon From Samples 96–10, 83–14, and 32–24

			Data for Wetherill Plot					Ages							Concordant Ages	
Sample	$^{207}Pb/^{206}Pb$	1σ abs	$207Pb/^{235}U$	1σ abs	$^{206}Pb/^{238}U$	1σ abs	Rho	$^{207}Pb/^{206}Pb$	1σ abs	$^{207}Pb/^{235}U$	1σ abs	$^{206}Pb/^{238}U$	1σ abs	% U-Pb disc	2σ abs	
NBP96–01-10																
Ju24c006	0.04812	0.00205	0.10124	0.00452	0.01520	0.00028	0.4	105	4	98	4	97	2	0,7	97	4
Ju24c007	0.47275	0.05707	2.81583	0.28924	0.04320	0.00328	0.7	4158	502	1360	140	273	21	79,9		
Ju24c008	0.05287	0.00336	0.41783	0.02678	0.05681	0.00123	0.3	323	21	354	23	356	8	−0,5	356	15
Ju24c009	0.08423	0.00314	3.59811	0.14222	0.30914	0.00617	0.5	1298	48	1549	61	1,736	35	−12,1		
Ju24c010	0.06023	0.00576	0.91774	0.08702	0.10951	0.00309	0.3	612	59	661	63	670	19	−1,3	670	36
Ju24c011	0.04746	0.00696	0.11918	0.01740	0.01822	0.00048	0.2	72	11	114	17	116	3	−1,8	116	6
Ju24c013	0.04772	0.00319	0.10889	0.00733	0.01655	0.00032	0.3	85	6	105	7	106	2	−0,8	106	4
Ju24c014	0.04632	0.00204	0.10724	0.00490	0.01679	0.00028	0.4	14	1	103	5	107	2	−3,8		
Ju24c015	0.05641	0.00244	0.43750	0.01963	0.05637	0.00108	0.4	469	20	368	17	354	7	4,1		
Ju24c016	0.04784	0.00597	0.11848	0.01469	0.01797	0.00046	0.2	91	11	114	14	115	3	−1,0	115	6
Ju24c017	0.04836	0.00245	0.11545	0.00600	0.01732	0.00032	0.4	117	6	111	6	111	2	0,2	111	4
Ju24c018	0.79643	0.05074	8.90714	0.46764	0.08095	0.00381	0.9	4915	313	2329	122	502	24	78,5		
Ju24c019	0.04828	0.00234	0.11413	0.00568	0.01715	0.00030	0.4	113	5	110	5	110	2	0,1	110	4
Ju24c020	0.04730	0.00852	0.10676	0.01913	0.01637	0.00047	0.2	64	12	103	18	105	3	−1,6	105	6
Ju24c021	0.04677	0.00379	0.11172	0.00905	0.01733	0.00038	0.3	37	3	108	9	111	2	−3,0		
Ju24c022	0.77456	0.04336	7.67018	0.35705	0.07167	0.00293	0.9	4876	273	2193	102	446	18	79,7		
Ju24c023	0.19107	0.00808	0.64240	0.02690	0.02440	0.00055	0.5	2751	116	504	21	155	4	69,2		
Ju24c024	0.04765	0.00277	0.11118	0.00651	0.01694	0.00033	0.3	82	5	107	6	108	2	−1,2	108	4
Ju24c025	0.05451	0.00460	0.49118	0.04124	0.06544	0.00164	0.3	392	33	406	34	409	10	−0,7	409	20
Ju24c026	0.07019	0.00264	0.15452	0.00612	0.01597	0.00029	0.5	934	35	146	6	102	2	30,0		
Ju24c030	0.07454	0.00263	1.86818	0.07013	0.18211	0.00335	0.5	1056	37	1070	40	1,078	20	−0,8		
Ju24c031	0.76567	0.04094	432.45984	438.15154	4.09573	4.14873	1.0	4859	260	6165	6246	10,497	10,633	−70,3		
Ju24c032	0.05569	0.00412	0.13753	0.01016	0.01790	0.00038	0.3	440	33	131	10	114	2	12,6		
Ju24c033	0.05862	0.00206	0.13641	0.00509	0.01688	0.00028	0.4	553	19	130	5	108	2	16,9		
Ju24c034	0.05085	0.00716	0.23600	0.03241	0.03339	0.00110	0.2	234	33	215	30	212	7	1,6	212	14
Ju24c035	0.10233	0.00465	4.12272	0.18671	0.29335	0.00648	0.5	1667	76	1659	75	1,658	37	0,0	1658	59
Ju24c036	0.04796	0.00449	0.13504	0.01261	0.02043	0.00046	0.2	97	9	129	12	130	3	−1,4	130	6
Ju24c037	0.07814	0.00222	2.07500	0.06474	0.19297	0.00339	0.6	1150	33	1141	36	1,137	20	0,3	1138	35
Ju24c038	0.05003	0.00426	0.14273	0.01209	0.02070	0.00047	0.3	196	17	135	11	132	3	2,5	132	6
Ju24c039	0.29417	0.00827	0.94265	0.02764	0.02322	0.00046	0.7	3440	97	674	20	148	3	78,1		
Ju24c040	0.07840	0.00245	2.00370	0.06559	0.18614	0.00315	0.5	1157	36	1117	37	1,100	19	1,5	1104	33
Ju24c041	0.05373	0.00308	0.41583	0.02399	0.05628	0.00112	0.3	360	21	353	20	353	7	0,0	353	14
Ju24c042	0.36433	0.01398	1.73529	0.06349	0.03451	0.00084	0.7	3768	145	1022	37	219	5	78,6		
Ju24c043	0.29489	0.01442	1.08758	0.04966	0.02670	0.00073	0.6	3444	168	747	34	170	5	77,3		
Ju24c044	0.04946	0.00445	0.16793	0.01501	0.02460	0.00055	0.3	170	15	158	14	157	4	0,6	157	7
Ju24c045	0.04726	0.00330	0.10056	0.00694	0.01543	0.00032	0.3	62	4	97	7	99	2	−1,5	99	4
Ju24c046	0.08743	0.00698	1.53138	0.11971	0.12718	0.00349	0.4	1370	109	943	74	772	21	18,2		
Ju24c047	0.07691	0.00391	1.93481	0.09883	0.18256	0.00372	0.4	1119	57	1093	56	1,081	22	1,1		
Ju24d006	0.73272	0.03208	8.06137	0.28038	0.0798	0.00264	1	4796	210	2238	78	495	16	77,9		
Ju24d007	0.04967	0.01235	0.15379	0.03775	0.02239	0.00098	0.2	180	45	145	36	143	6	1,7	143	12
Ju24d008	0.04933	0.00219	0.14921	0.0065	0.02188	0.00038	0.4	164	7	141	6	140	2	1,2	140	5
Ju24d009	0.04943	0.00375	0.11192	0.00835	0.01643	0.00033	0.3	168	13	108	8	105	2	2,5	105	4
Ju24d010	0.08389	0.01058	0.20253	0.02467	0.01743	0.00064	0.3	1290	163	187	23	111	4	40,5		
Ju24d011	0.05236	0.00659	0.10792	0.0133	0.01524	0.00047	0.2	301	38	104	13	98	3	6,3		
Ju24d012	0.08967	0.00210	0.27716	0.0064	0.02241	0.00035	0.7	1419	33	248	6	143	2	42,5		
Ju24d013	0.04846	0.00529	0.11856	0.01265	0.01772	0.00048	0.3	122	13	114	12	113	3	0,5	113	6
Ju24d014	0.17770	0.00541	1.74246	0.05007	0.07112	0.00131	0.6	2632	80	1024	29	443	8	56,8		
Ju24d015	0.04818	0.00274	0.11791	0.00657	0.0178	0.00032	0.3	108	6	113	6	114	2	−0,5	114	4
Ju24d016	0.04810	0.00261	0.1117	0.00597	0.01684	0.0003	0.3	104	6	108	6	108	2	−0,1	108	4
Ju24d017	0.05182	0.00579	0.15746	0.01725	0.02286	0.00065	0.3	277	31	148	16	146	4	1,9	146	8
Ju24d018	0.05300	0.00687	0.13189	0.01674	0.01909	0.00061	0.3	329	43	126	16	122	4	3,1		

Table 3. (continued)

	Data for Wetherill Plot							Ages							Concordant Ages	
Sample	$^{207}Pb/^{206}Pb$	1σ abs	$207Pb/^{235}U$	1σ abs	$^{206}Pb/^{238}U$	1σ abs	Rho	$^{207}pb/^{206}pb$	1σ abs	$^{207}Pb/^{235}U$	1σ abs	$^{206}pb/^{238}U$	1σ abs	% U-Pb disc	2σ abs	
Ju24d019	0.09781	0.00492	0.21921	0.01061	0.01626	0.00034	0.4	1583	80	201	10	104	2	48,3		
Ju24d020	0.05434	0.00216	0.42226	0.0165	0.05715	0.00097	0.4	385	15	358	14	358	6	−0,2	358	12
Ju24d021	0.04924	0.00208	0.12144	0.00501	0.01793	0.0003	0.4	159	7	116	5	115	2	1,6	115	4
Ju24d022	0.04824	0.00291	0.1064	0.00628	0.01612	0.00031	0.3	111	7	103	6	103	2	−0,4	104	4
Ju24d023	0.06480	0.00306	0.21161	0.00978	0.02369	0.00043	0.4	768	36	195	9	151	3	22,6		
Ju24d024	0.20253	0.04199	0.47512	0.09079	0.01953	0.00161	0.4	2847	590	395	75	125	10	68,4		
Ju24d025	0.04819	0.00123	0.11646	0.003	0.01761	0.00028	0.6	109	3	112	3	113	2	−0,6	113	4
Ju24d026	0.04739	0.00327	0.15049	0.01019	0.02303	0.00047	0.3	69	5	142	10	147	3	−3,1		
Ju24d027	0,07665	0,00330	1,85064	0,078	0,17695	0,00346	0,5	1112	48	1064	45	1,050	21	1,3		
Ju24d032	0,13112	0,00719	0,11963	0,00623	0,00662	0,00015	0,4	2113	116	115	6	43	1	62,9		
Ju24d033	0,13351	0,00195	7,31453	0,10443	0,39511	0,00549	1	2145	31	2151	31	2,146	30	0,2	2154	11
Ju24d034	0,05845	0,00140	0,73906	0,01729	0,09161	0,00131	0,6	547	13	562	13	565	8	−0,6	564	15
Ju24d035	0,05921	0,00399	0,76221	0,05028	0,09367	0,00202	0,3	575	39	575	38	577	12	−0,3	577	24
Ju24d036	0,07115	0,00123	1,59366	0,02782	0,16248	0,00241	0,8	962	17	968	17	971	14	−0,3	967	22
Ju24d037	0,33504	0,01526	1,32588	0,05269	0,02871	0,00078	0,7	3640	166	857	34	182	5	78,7		
Ju24d038	0,06183	0,00148	0,67829	0,0161	0,07962	0,00122	0,6	668	16	526	12	494	8	6,1		
Ju24d039	0,73196	0,06492	22,21374	2,75323	0,22048	0,02707	1	4795	425	3193	396	1,284	158	59,8		
Ju24d040	0,04838	0,00384	0,11313	0,00876	0,01699	0,00037	0,3	118	9	109	8	109	2	0,2	109	5
Ju24d041	0,04830	0,00382	0,12234	0,00949	0,01838	0,00041	0,3	114	9	117	9	117	3	−0,2	117	5
Ju24d042	0,04762	0,00323	0,10902	0,00726	0,0168	0,00036	0,3	80	5	105	7	107	2	−2,2	107	5
Ju24d043	0,04888	0,00142	0,11107	0,0032	0,01649	0,00025	0,5	142	4	107	3	105	2	1,4	106	3
Ju24d044	0,04973	0,00226	0,15423	0,00686	0,02258	0,0004	0,4	182	8	146	6	144	3	1,2	144	5
Ju24d045	0,05049	0,00135	0,12026	0,00318	0,01728	0,00027	0,6	218	6	115	3	110	2	4,2		
Ju24d046	0,05352	0,00130	0,41637	0,01	0,05644	0,00085	0,6	351	8	353	8	354	5	−0,1	354	10
Ju24d047	0,05802	0,00215	0,69651	0,02522	0,08718	0,00146	0,5	531	20	537	19	539	9	−0,4	539	17
Ju24d048	0,24641	0,01135	0,73239	0,03049	0,02152	0,00054	0,6	3162	146	558	23	137	3	75,4		
Ju24d050	0,04861	0,00264	0,11794	0,00627	0,01762	0,00031	0,3	129	7	113	6	113	2	0,5	113	4
Ju24d051	0,04770	0,00222	0,11246	0,00514	0,01711	0,00029	0,4	84	4	108	5	109	2	−1,1	110	4
Ju24d052	0,05163	0,00435	0,11189	0,00921	0,01571	0,00037	0,3	269	23	108	9	100	2	6,7		
DF83–014																
Ju25e006	0.07663	0.00289	1.89073	0.08115	0.17908	0.00341	0.4	1112	42	1078	46	1,062	20	1,5		
Ju25e007	0.04767	0.00772	0.14795	0.02367	0.02254	0.00086	0.2	83	13	140	22	144	5	−2,6		
Ju25e008	0.08022	0.00886	0.22583	0.02453	0.02045	0.00069	0.3	1202	133	207	22	130	4	36.9		
Ju25e009	0.06970	0.00543	0.16619	0.01305	0.01732	0.00044	0.3	920	72	156	12	111	3	29.1		
Ju25e010	0.41504	0.02194	3.12259	0.15601	0.05476	0.00185	0.7	3964	210	1438	72	344	12	76.1		
Ju25e011	0.08333	0.00787	0.26811	0.02524	0.02337	0.00067	0.3	1277	121	241	23	149	4	38.3		
Ju25e012	0.05459	0.00324	0.39457	0.02436	0.05259	0.00115	0.4	395	23	338	21	330	7	2.2	331	14
Ju25e014	0.04963	0.00452	0.12437	0.01138	0.01825	0.00049	0.3	178	16	119	11	117	3	2.0	117	6
Ju25e015	0.04881	0.00363	0.10928	0.00832	0.01619	0.00036	0.3	139	10	105	8	104	2	1.7	104	5
Ju25e016	0.04705	0.00206	0.10035	0.00484	0.01549	0.00027	0.4	52	2	97	5	99	2	−2.0	99	4
Ju25e017	0.05885	0.00259	0.73612	0.03553	0.09083	0.00168	0.4	562	25	560	27	560	10	−0.1	560	20
Ju25e018	0.05862	0.00223	0.70439	0.03042	0.08727	0.00158	0.4	553	21	541	23	539	10	0.4	540	19
Ju25e019	0.05639	0.00176	0.61203	0.02307	0.07884	0.00135	0.5	468	15	485	18	489	8	−0.9	489	16
Ju25e020	0.04775	0.00175	0.11516	0.00485	0.01751	0.00031	0.4	87	3	111	5	112	2	−1.1	112	4
Ju25e021	0.06153	0.00277	0.90585	0.04448	0.10670	0.00198	0.4	658	30	655	32	654	12	0.2	654	23
Ju25e022	0.05121	0.00743	0.11889	0.01719	0.01686	0.00050	0.2	250	36	114	16	108	3	5.5		
Ju25e023	0.06167	0.00152	1.36421	0.04452	0.16069	0.00259	0.5	663	16	874	29	961	15	−9.9		
Ju25e024	0.05871	0.00211	0.73198	0.03035	0.09054	0.00160	0.4	556	20	558	23	559	10	−0.2	559	19
Ju25e025	0.07608	0.00216	1.93261	0.06859	0.18443	0.00314	0.5	1097	31	1092	39	1,091	19	0.1	1091	33
Ju25e026	0.06406	0.00213	1.06193	0.04142	0.12066	0.00223	0.5	744	25	735	29	734	14	0.1	734	25
Ju25e027	0.05872	0.00160	1.19944	0.04143	0.14847	0.00248	0.5	557	15	800	28	892	15	−11.5		
Ju25e028	0.05716	0.00322	0.63172	0.03688	0.08045	0.00183	0.4	498	28	497	29	499	11	−0.3	499	22
Ju25e029	0.04904	0.00316	0.09900	0.00651	0.01468	0.00035	0.4	150	10	96	6	94	2	2.0	94	5

AGU Geochemistry, Geophysics, Geosystems

10.1002/2016GC006728

Table 3. (continued)

	Data for Wetherill Plot							Ages							Concordant Ages	
Sample	$^{207}Pb/^{206}Pb$	1σ abs	207Pb/^{235}U	1σ abs	$^{206}Pb/^{238}U$	1σ abs	Rho	$^{207}pb/^{206}pb$	1σ abs	$^{207}Pb/^{235}U$	1σ abs	$^{206}pb/^{238}U$	1σ abs	% U-Pb disc	2σ abs	
Ju25e030	0.18379	0.00461	1.48129	0.04881	0.05850	0.00097	0.5	2687	67	923	30	366	6	60.3		
Ju25e031	0.06907	0.00231	1.44448	0.05716	0.15172	0.00260	0.4	901	30	908	36	911	16	−0.3	910	29
Ju25e032	0.06772	0.00190	1.34569	0.04715	0.14421	0.00236	0.5	860	24	866	30	868	14	−0.3	868	26
Ju25e033	0.07544	0.00286	1.90099	0.08152	0.18284	0.00339	0.4	1080	41	1081	46	1,082	20	−0.1		
Ju25e037	0.04911	0.00184	0.12891	0.00552	0.01904	0.00032	0.4	153	6	123	5	122	2	1.2	122	4
Ju25e038	0.05743	0.00186	0.63985	0.02462	0.08077	0.00134	0.4	508	16	502	19	501	8	0.3	501	16
Ju25e039	0.07465	0.00186	1.38099	0.04529	0.13412	0.00214	0.5	1059	26	881	29	811	13	7.9		
Ju25e040	0.05536	0.00173	0.55221	0.02076	0.07228	0.00124	0.5	427	13	446	17	450	8	−0.8	450	15
Ju25e041	0.05834	0.00187	0.72184	0.02757	0.08969	0.00149	0.4	543	17	552	21	554	9	−0.4	554	17
Ju25e042	0.05050	0.00230	0.20787	0.01032	0.02983	0.00054	0.4	218	10	192	10	189	3	1.2	189	7
Ju25e043	0.06299	0.00200	0.74018	0.02810	0.08523	0.00138	0.4	708	22	563	21	527	9	6.3		
Ju25e044	0.04670	0.00227	0.13694	0.00717	0.02125	0.00038	0.3	34	2	130	7	136	2	−4.0		
Ju25e045	0.06912	0.00198	1.43724	0.05115	0.15052	0.00252	0.5	902	26	905	32	904	15	0.1	904	28
Ju25e046	0.07788	0.00216	0.66339	0.02311	0.06169	0.00100	0.5	1144	32	517	18	386	6	25.3		
Ju25e047	0.05016	0.00631	0.10960	0.01378	0.01584	0.00042	0.2	202	25	106	13	101	3	4.1		
Ju25e048	0.05298	0.00264	0.41489	0.02222	0.05676	0.00106	0.3	328	16	352	19	356	7	−1.0	356	13
Ju25e049	0.05661	0.00164	0.61162	0.02196	0.07816	0.00128	0.5	476	14	485	17	485	8	−0.1	485	15
Ju25e050	0.09015	0.00224	2.14094	0.06995	0.17212	0.00266	0.5	1429	35	1162	38	1,024	16	11.9		
Ju25e051	0.06386	0.00557	0.13812	0.01216	0.01565	0.00037	0.3	737	64	131	12	100	2	23.8		
Ju25e052	0.04914	0.00248	0.10900	0.00591	0.01606	0.00028	0.3	155	8	105	6	103	2	2.2	103	4
Ju25e053	0.05326	0.00139	0.37930	0.01279	0.05155	0.00080	0.5	340	9	327	11	324	5	0.8	324	10
Ju25e054	0.07849	0.00243	2.17402	0.08035	0.19879	0.00343	0.5	1159	36	1173	43	1,169	20	0.3	1170	36
Ju25e055	0.37190	0.02549	6.64725	0.42214	0.12862	0.00560	0.7	3799	260	2066	131	780	34	62.2		
Ju25e056	0.07894	0.00204	2.17142	0.07267	0.19888	0.00314	0.5	1171	30	1172	39	1,169	18	0.2	1170	32
Ju25e057	0.06652	0.00223	1.31273	0.05138	0.14241	0.00245	0.4	823	28	851	33	858	15	−0.8	857	27
Ju25e058	0.05701	0.00280	0.64171	0.03355	0.08085	0.00156	0.4	492	24	503	26	501	10	0.4	501	19
Ju25e059	0.06516	0.00188	0.58702	0.02092	0.06512	0.00104	0.4	780	22	469	17	407	6	13.3		
Ju25e060	0.26389	0.01508	0.99013	0.05474	0.02690	0.00080	0.5	3270	187	699	39	171	5	75.5		
Ju25e061	0.05520	0.00272	0.52178	0.02692	0.06843	0.00124	0.4	420	21	426	22	427	8	−0.1	427	15
Ju25e062	0.25789	0.01669	4.48268	0.28580	0.12560	0.00424	0.5	3234	209	1728	110	763	26	55.9		
Ju25e063	0.06931	0.00188	1.42350	0.04857	0.14892	0.00229	0.5	908	25	899	31	895	14	0.4	895	25
Ju25e064	0.04783	0.00383	0.10342	0.00829	0.01558	0.00036	0.3	91	7	100	8	100	2	0.3	100	5
Ju25c005_91500	0.07538	0.00401	1.87954	0.09612	0.17943	0.00467	0.5	1079	57	1074	55	1,064	28	0.9		
Ju25c006	0.04939	0.01191	0.13329	0.03163	0.01980	0.00094	0.2	166	40	127	30	126	6	0.5	126	12
Ju25c007	0.07829	0.01359	0.26142	0.04432	0.02424	0.00104	0.3	1154	200	236	40	154	7	34.5		
Ju25c008	0.08615	0.00377	0.18207	0.00765	0.01536	0.00036	0.6	1342	59	170	7	98	2	42.1		
Ju25c009	0.07713	0.00596	0.17172	0.01276	0.01620	0.00047	0.4	1125	87	161	12	104	3	35.6		
Ju25c010	0.13442	0.00284	7.40510	0.15024	0.39987	0.00822	1.0	2157	46	2162	44	2,168	45	−0.3	2155	10
Ju25c011	0.07215	0.00204	1.61677	0.04427	0.16314	0.00348	0.8	990	28	977	27	9,74	21	0.3	976	34
Ju25c012	0.07514	0.00173	1.85792	0.04125	0.17945	0.00367	0.9	1072	25	1066	24	1,064	22	0.2	1068	26
Ju25c013	0.17255	0.00617	0.44130	0.01458	0.01859	0.00044	0.7	2583	92	371	12	119	3	68.0		
Ju25c014	0.05201	0.00190	0.28301	0.01004	0.03956	0.00086	0.6	286	10	253	9	250	5	1.2	250	11
Ju25c015	0.05789	0.00139	0.67547	0.01589	0.08462	0.00175	0.9	526	13	524	12	524	11	0.1	524	19
Ju25c016	0.64850	0.02156	8.94317	0.25083	0.10009	0.00283	1.0	4621	154	2332	65	615	17	73.6		
Ju25c017	0.04702	0.02891	0.12551	0.07646	0.01933	0.00167	0.1	50	31	120	73	123	11	−2.8		
Ju25c018	0.03746	0.00849	0.12552	0.02816	0.02430	0.00093	0.2	−523	−119	120	27	155	6	−28.9		
Ju25c019	0.07665	0.00220	1.97291	0.05429	0.18695	0.00394	0.8	1112	32	1106	30	1,105	23	0.1	1106	37
Ju25c020	0.35612	0.01403	1.67001	0.05782	0.03403	0.00093	0.8	3733	147	997	35	216	6	78.4		
Ju25c021	0.06806	0.00154	1.33494	0.02913	0.14217	0.00292	0.9	870	20	861	19	857	18	0.5	865	23
Ju25c022	0.04879	0.00351	0.12473	0.00870	0.01849	0.00047	0.4	138	10	119	8	118	3	1.0	118	6
Ju25c028	0.07570	0.00173	1.95465	0.04272	0.18713	0.00385	0.9	1087	25	1100	24	1,106	23	−0.5	1094	24
Ju25c029	0.07755	0.00366	2.08569	0.09493	0.19444	0.00469	0.5	1135	54	1144	52	1,145	28	−0.1	1145	48
Ju25c030	0.06063	0.00165	0.85666	0.02244	0.10253	0.00211	0.8	626	17	628	16	629	13	−0.1	629	23

AGU Geochemistry, Geophysics, Geosystems

10.1002/2016GC006728

Geochemistry, Geophysics, Geosystems

10.1002/2016GC006728

Table 3. (continued)

			Data for Wetherill Plot					Ages							Concordant Ages	
Sample	$^{207}Pb/^{206}Pb$	1σ abs	207Pb/^{235}U	1σ abs	$^{206}Pb/^{238}U$	1σ abs	Rho	$^{207}pb/^{206}pb$	1σ abs	$^{207}Pb/^{235}U$	1σ abs	$^{206}pb/^{238}U$	1σ abs	% U-Pb disc	2σ abs	
Ju25c031	0.11648	0.00972	0.34729	0.02731	0.02165	0.00075	0.4	1903	159	303	24	138	5	54.4		
Ju25c032	0.07094	0.00202	1.57165	0.04267	0.16069	0.00335	0.8	956	27	959	26	961	20	−0.2	960	33
Ju25c033	0.05907	0.00173	0.75431	0.02111	0.09258	0.00189	0.7	570	17	571	16	571	12	0.0	571	22
Ju25c034	0.07520	0.00238	1.87339	0.05676	0.18051	0.00389	0.7	1074	34	1072	32	1,070	23	0.2	1071	38
Ju25c035	0.05755	0.00133	0.67029	0.01482	0.08449	0.00170	0.9	513	12	521	12	523	10	−0.4	521	18
Ju25c036	0.04768	0.01616	0.14223	0.04782	0.02170	0.00105	0.1	83	28	135	45	138	7	−2.5		
Ju25c037	0.18861	0.01772	0.47584	0.04130	0.01833	0.00076	0.5	2730	256	395	34	117	5	70.4		
Ju25c038	0.02325	0.00401	0.06230	0.01068	0.01944	0.00051	0.2	−2024	−349	61	11	124	3	−102.3		
Ju25c039	0.05637	0.00214	0.57112	0.02059	0.07383	0.00159	0.6	467	18	459	17	459	10	−0.1	459	19
Ju25c040	0.64151	0.02764	12.93097	0.47426	0.14666	0.00523	1.0	4605	198	2675	98	882	31	67.0		
Ju25c041	0.04806	0.00469	0.12430	0.01188	0.01878	0.00053	0.3	102	10	119	11	120	3	−0.8	120	7
Ju25c042	0.07589	0.00250	0.42228	0.01328	0.04045	0.00086	0.7	1092	36	358	11	256	5	28.5		
Ju25c043	0.09983	0.00239	0.22404	0.00508	0.01633	0.00034	0.9	1621	39	205	5	104	2	49.1		
Ju25c044	0.10239	0.00221	0.89830	0.01830	0.06392	0.00133	1.0	1668	36	651	13	399	8	38.6		
Ju25c045	0.07305	0.00189	1.71279	0.04159	0.16973	0.00354	0.9	1015	26	1013	25	1,011	21	0.3	1014	31
Ju25c046	0.38961	0.02026	1.77963	0.07868	0.03334	0.00115	0.8	3869	201	1038	46	211	7	79.6		
E LT 32–024																
Ma21a005	0.05854	0.00208	0.71942	0.02288	0.08874	0.00371	0.6	550	20	550	17	543	11	0,4	548	20
Ma21a006	0.05029	0.00351	0.20841	0.01397	0.03005	0.00056	0.3	203	15	132	13	191	4	0,7	131	8
Ma21a007	0.05699	0.00134	0.63556	0.01144	0.08111	0.00343	1.0	491	12	500	9	503	9	−0,6	493	12
Ma21a0D8	0.05826	0.00177	0.68025	0.01762	0.08480	0.00153	0.7	540	16	527	34	525	9	0,4	525	18
Ma21a009	0.09327	0.00202	1.11206	0.01719	0.08664	0.00355	1.2	1493	32	759	32	536	10	23,4		
Ma21a012	0.05733	0.00133	0.62186	0.01030	0.07887	0.00339	3.0	504	12	431	9	489	9	0,3	436	9
Ms21a013	0.09158	0.00205	3.23315	0.05478	0.25580	0.00459	3.0	1461	33	1465	25	1,463	27	−0,2	1462	8
Ma21a014	0.08634	0.00202	2.77391	0.04918	0.23205	0.00421	1.0	1357	32	1343	24	1,345	24	0,2	1353	9
Ma21a015	0.05726	0.00165	0.62924	0.01534	0.07383	0.00346	0.3	502	14	436	32	495	9	0,1	435	17
Ma21a016	0.06087	0.00622	0.84117	0.08339	0.10018	0.00287	0.3	635	65	620	61	615	18	0,7	616	34
Ma21a017	0.05703	0.00158	0.62610	0.01444	0.07970	0.00345	0.8	493	14	494	31	494	9	−0,1	434	17
Ma21a018	0.05676	0.00189	0.59464	0.01752	0.07598	0.00344	0.6	482	16	474	34	472	9	0,4	472	17
Ma21a013	0.09350	0.00241	3.92779	0.07553	0.28579	0.00540	1.0	1617	39	1613	31	1,620	31	−0,1	1618	13
Ma21a021	0.08802	0.00345	1.23061	0.04345	0.10146	0.00202	0.6	1383	51	815	29	623	12	23,5		
Ma21a022	0.05713	0.00211	0.63814	0.02118	0.08105	0.00354	0.6	437	18	501	37	502	10	−0,2	502	18
Ma21a024	0.05552	0.00167	0.21292	0.00548	0.02787	0.00050	0.7	433	13	196	5	177	3	9,6		
Ma21a026	0.08652	0.00164	1.02619	0.01217	0.08607	0.00152	1.5	1352	26	717	9	532	9	25,8		
Ma21a027	0.05760	0.00170	0.62657	0.01544	0.07914	0.00342	0.7	515	15	434	32	491	9	0,6	432	17
Ma21a028	0.07286	0.00289	0.81747	0.02330	0.08141	0.00352	0.6	1010	40	607	22	505	10	16,8		
Ma21a023	0.07755	0.00228	2.06016	0.05152	0.19253	0.00373	0.3	1138	33	1136	28	1,135	22	0,1	1136	34
Ma21a030	0.05992	0.00157	0.73214	0.01650	0.09474	0.00359	0.8	601	16	587	32	534	10	0,5	586	18
Ma21a031	0.07559	0.00204	1.91646	0.04253	0.13409	0.00339	0.3	1084	29	1037	24	1,083	20	0,2	1087	30
Ma21a032	0.07584	0.00269	1.89108	0.05961	0.18080	0.00358	0.6	1091	39	1078	34	1,071	21	0,6		
Ma21a036	0.06058	0.00437	0.24787	0.01709	0.02959	0.00073	0.4	624	45	225	35	189	5	16,1		
Ma21a037	0.05048	0.00616	0.23125	0.02778	0.03325	0.00079	0.2	217	26	213	25	211	5	0,2	211	10
Ma21a038	0.06051	0.00139	0.66999	0.01183	0.08036	0.00345	1.0	622	14	521	9	438	9	4,3		
Ma21a039	0.05745	0.00219	0.66877	0.02329	0.08444	0.00368	0.6	509	19	520	38	523	10	−0,5	522	20
Ma21a040	0.05181	0.00267	0.29789	0.01446	0.04172	0.00087	0.4	277	14	265	33	263	5	0,5	264	11
Ma21a041	0.04956	0.00600	0.11968	0.01410	0.01752	0.00053	0.3	174	21	115	34	112	3	2,5		
Ma21a042	0.06112	0.00232	0.86809	0.02987	0.10304	0.00205	0.6	643	24	635	22	632	13	0,4	633	24
Ma21a043	0.04694	0.00209	0.20322	0.00802	0.03013	0.00058	0.5	145	6	188	7	138	4	−1,9	131	7
Ma21a044	0.13734	0.00623	0.32614	0.01328	0.01722	0.00040	0.6	2194	39	287	32	110	3	61,6		
Ma21a045	0.05068	0.00372	0.23918	0.01696	0.03426	0.00074	0.3	226	17	218	35	217	5	0,3	217	9
Ma21a046	0.05792	0.00171	0.66583	0.01681	0.08338	0.00353	0.7	527	16	518	33	516	9	0,4	517	18
Ma21a047	0.07755	0.00221	2.04361	0.04301	0.19106	0.00368	0.3	1138	32	1130	27	1,127	22	0,3	1130	33
Ma21a048	0.05893	0.00210	0.71681	0.02295	0.08832	0.00369	0.6	565	20	549	38	546	10	0,6	546	20

AGU Geochemistry, Geophysics, Geosystems

10.1002/2016GC006728

Table 3. (continued)

			Data for Wetherill Plot					Ages							Concordant Ages	
Sample	$^{207}Pb/^{206}Pb$	1σ abs	207Pb/^{235}U	1σ abs	$^{206}Pb/^{238}U$	1σ abs	Rho	$^{207}pb/^{206}pb$	1σ abs	$^{207}Pb/^{235}U$	1σ abs	$^{206}pb/^{238}U$	1σ abs	% U-Pb disc	2σ abs	
Ma21a049	0.07237	0.D0341	1.67075	0.07235	0.16808	0.00375	0.5	996	47	997	43	1,002	22	−0,4	1001	40
Ma21a050	0.07742	0.00201	2.06705	0.04326	0.19359	0.00354	0.3	1132	29	1138	24	1,141	21	−0,2	1137	28
Ma21a051	0.07095	0.00175	1.55857	0.02336	0.15356	0.00285	0.3	956	24	954	33	954	17	0,0	354	21
Ma21a052	0.06006	0.00173	0.83133	0.02024	0.10041	0.00383	0.7	606	17	614	35	617	11	−0,4	616	20
Ma21a053	0.05892	0.00149	0.73737	0.01438	0.09072	0.00357	0.3	564	14	561	31	560	10	0,2	561	17
Ma23a054	0.11930	0.00262	1.25012	0.01332	0.07599	0.00338	1.3	1946	43	823	33	472	9	42,7		
Ma21a055	0.05905	0.00191	0.72717	0.02057	0.08942	0.00372	0.7	569	18	555	36	582	11	0,5	553	20
Ma21a056	0.05722	0.00185	0.6113D	0.01750	0.07816	0.00351	0.7	500	16	484	34	485	9	−0,2	485	18
Ma21a057	0.05386	0.00217	0.46279	0.01685	0.06257	0.00339	0.5	365	15	336	34	331	7	−1,3	331	14
Ma21a058	0.25172	0.02299	0.05149	0.00425	0.00149	0.00006	0.5	3196	232	51	4	10	0	31,2		
Ma21a059	0.05820	0.00258	0.68279	0.02803	0.08542	0.00376	0.5	537	24	528	22	523	11	0,0	528	31
Ma21a060	0.06545	0.00155	1.14308	0.02056	0.12711	0.00223	1.0	783	19	774	34	771	14	0,3	778	14
Ma21a061	0.05084	0.D0323	0.25633	0.01549	0.03682	0.00084	0.4	234	15	232	14	233	5	−0,6	233	10
Ma21aOG2	0.05221	0.00306	0.31318	0.01740	0.04354	0.00091	0.4	295	17	277	15	275	6	0,5	275	11
Ma21a065	0.08320	0.00437	2.51919	0.12386	0.21953	0.00491	0.5	1274	67	1273	63	1,279	29	−0,1	1273	50
Ma21a06B	0.07398	0.00170	1.73666	0.03055	0.17038	0.00323	1.0	1041	24	1022	38	1,018	13	0,5	3030	8
Ma21a067	0.04725	0.00664	0.03934	0.00542	0.00602	0.00015	0.2	62	3	33	5	39	1	0,8	33	2
Ma23a068	0.05750	0.00155	0.67061	0.01439	0.08443	0.00352	0.3	515	14	521	32	523	9	−0,3	522	17
Ma21b005	0.07590	0.00329	1.86493	0.07396	0.17810	0.00300	0.4	1092	47	1063	42	1,057	13	1,1		
Ma21b006	0.02098	0.00309	0.05126	0.00746	0.01772	0.00039	0.2	−2431	−358	51	7	113	2	−123,1		
Ma21h007	0.05958	0.00157	0.73354	0.01645	0.08926	0.00328	0.6	588	16	559	33	551	8	1,3	553	15
Ma21b008	0.05747	0.00227	0.68756	0.02493	0.08675	0.00338	0.4	510	20	531	39	536	9	−0,9	536	16
Ma21b009	0.05819	0.00198	0.72161	0.02229	0.08989	0.00339	0.5	537	18	552	37	555	9	−0,6	555	16
Ma21b010	0.07155	0.00340	0.25133	0.01119	0.02542	0.00044	0.4	976	46	228	30	162	3	28,3		
Ma21b0JI	0.05830	0.00259	0.68972	0.02863	0.08556	0.00345	0.4	541	24	533	22	530	9	0,5	530	17
Ma21b012	0.10714	0.00672	0.38401	0.02264	0.02601	0.00056	0.4	1751	110	330	39	166	4	43,8		
Ma21b013	0.07622	0.00230	1.97950	0.05277	0.18818	0.00285	0.6	1101	33	1109	30	1,112	17	0,3	1111	29
Ma21b014	0.06617	0.00195	1.22674	0.03214	0.13446	0.00200	0.6	812	24	813	21	813	12	0,0	313	22
Ma21b015	0.05850	0.00183	0.69846	0.01358	0.08646	0.00330	0.5	552	17	538	35	535	8	0,6	535	15
Ma21b016	0.05859	0.00213	0.70340	0.02326	0.08711	0.00333	0.5	552	20	541	38	533	8	0,4	539	16
Ma21b017	0.04728	0.00287	0.11313	0.00660	0.01735	0.00030	0.3	53	4	109	6	111	2	−1,3	111	4
Ma21b018	0.07057	0.00177	1.55805	0.03249	0.16010	0.00226	0.7	945	24	954	20	957	14	−0,4	956	23
Ma21b019	0.06003	0.00400	0.78965	0.05085	0.09536	0.00380	0.3	605	40	591	38	587	11	0,6	587	21
Ma21b02G	0.06028	0.D0154	0.85249	0.01829	0.10259	0.00345	0.7	614	16	626	13	630	9	−0,6	629	16
Ma21b021	0.05158	0.01457	0.29683	0.08272	0.04165	0.00389	0.2	271	77	264	74	263	12	0,3	263	23
Ma21b022	0.04908	0.00144	0.18903	0.00483	0.02794	0.00040	0.6	152	4	176	4	173	3	−1,0	178	5
Ma21b023	0.06194	0.00449	0.93594	0.06510	0.10954	0.00237	0.3	672	49	671	47	671	15	0,0	671	27
Ma21b024	0.06307	0.00335	1.00963	0.05119	0.11612	0.00203	0.3	711	38	709	36	708	12	0,1	708	23
Ma21b025	0.07456	0.00228	1.81132	0.04307	0.17604	0.00255	0.6	1059	32	1050	28	1,045	16	0,4	1047	28
Ma21b02G	0.04829	0.00339	0.11545	0.00785	0.01734	0.00030	0.3	114	8	111	8	111	2	0,1	111	4
Ma21b027	0.05031	0.D0253	0.20551	0.00982	0.02965	0.00048	0.3	209	11	190	9	188	3	0,7	188	6
Ma21b028	0.06044	0.00239	0.49769	0.01816	0.05975	0.00094	0.4	613	24	410	35	374	6	8,8		
Ma21b029	0.049B3	0.00327	0.19955	0.01257	0.02307	0.00054	0.3	187	12	185	32	185	3	0,0	185	7
Ma21b030	0.03356	0.00203	0.26072	0.01513	0.05619	0.00093	0.3	−819	−43	235	34	352	6	−19,8		
Ma21b031	0.08866	0.00283	1.34980	0.05679	0.15968	0.00250	0.6	1397	45	1038	32	955	16	13,1		
Ma21b032	0.07303	0.00203	1.70674	0.04061	0.16951	0.00246	0.6	1015	28	1011	24	1,009	15	0,2	1010	26
Ma21h033	0.04935	0.00393	0.18039	0.01397	0.02652	0.00052	0.3	164	13	168	33	169	3	−0,2	169	7
Ma21b035	0.07457	0.00201	1.82303	0.04123	0.17713	0.00248	0.6	1060	29	1054	24	1,051	15	0,2	1052	25
MB21KJ39	0.05059	0.00300	0.23845	0.01354	0.03418	0.00052	0.3	222	13	217	32	217	4	0,2	217	8
Ma21b040	0.07340	0.00244	0.75720	0.02275	0.07486	0.00315	0.5	1025	34	572	37	465	7	18,7		
Ma21b041	0.05705	0.00194	0.64089	0.01386	0.08147	0.00322	0.5	433	17	503	35	505	8	−0,4	505	14
Ma21b042	0.13252	0.00298	4.70048	0.03404	0.25732	0.00358	0.3	2132	48	1767	32	1,476	21	16,5		
Ma21b043	0.08054	0.D0242	2.32140	0.06154	0.20874	0.00313	0.6	1213	36	1219	32	1,222	18	0,3	1221	31

AGU Geochemistry, Geophysics, Geosystems

10.1002/2016GC006728

Table 3. (continued)

			Data for Wetherill Plot					Ages							Concordant Ages	
Sample	$^{207}Pb/^{206}Pb$	1σ abs	207Pb/^{235}U	1σ abs	$^{206}Pb/^{238}U$	1σ abs	Rho	$^{207}Pb/^{206}Pb$	1σ abs	$^{207}Pb/^{235}U$	1σ abs	$^{206}Pb/^{238}U$	1σ abs	% U-Pb disc	2σ abs	
Ma21b044	0.07453	0.00234	0.83065	0.02310	0.08039	0.00120	0.5	1067	33	614	17	493	7	18,8		
Ma21b045	0.05753	0.00234	0.67158	0.02541	0.08445	0.00133	0.4	516	21	522	20	523	8	−0,2	523	15
Ma21b046	0.05930	0.00403	0.72483	0.04743	0.08855	0.00187	0.3	578	39	554	36	548	12	1,1	548	22
Ma21b047	0.07941	0.00321	2.21243	0.08172	0.20185	0.00340	0.5	1182	48	1185	44	1,185	20	0,0	1185	35
Ma21b048	0.06107	0.00208	0.90140	0.02777	0.10706	0.00153	0.5	642	22	652	20	656	10	−0,5	655	19
Ma21b049	0.04996	0.00647	0.19523	0.02475	0.02848	0.00080	0.2	193	25	181	23	181	5	0,0	181	10
Ma21b050	0.05018	0.00342	0.21821	0.01436	0.03154	0.00058	0.3	203	14	200	13	200	4	0,1	200	7
Ma21b051	0.07824	0.00304	2.05539	0.07370	0.19157	0.00335	0.5	1153	45	1134	41	1,130	20	0,4	1131	35
Ma21b052	0.04877	0.02037	0.16646	0.06875	0.02439	0.00159	0.2	137	57	156	65	158	10	−1,4	158	20
Ma21b053	0.07380	0.00218	1.91048	0.04975	0.18771	0.00280	0.6	1036	31	1085	28	1,109	17	−2,2	1100	28
Ma21b054	0.05224	0.00285	0.31683	0.01650	0.04420	0.00080	0.3	296	16	279	15	279	5	0,2	279	10
Ma21b055	0.05855	0.00348	0.71325	0.04035	0.08814	0.00157	0.3	554	33	547	31	545	10	0,4	545	20
Ma21b056	0.06891	0.00230	0.67937	0.02045	0.07134	0.00110	0.5	896	30	526	16	444	7	15,6		
Ma21b057	0.08447	0.00323	0.89888	0.03129	0.07708	0.00127	0.5	1303	50	651	23	479	8	26,5		
Ma21b059	0.06580	0.00194	1.14429	0.02965	0.12722	0.00195	0.6	800	24	775	20	772	12	0,3	773	22
Ma21b0G0	0.11022	0.00262	4.87885	0.09618	0.32144	0.00470	0.7	1803	43	1799	35	1,797	26	0,1	1799	33
Ma21b051	0.07954	0.00360	2.26180	0.09458	0.20558	0.00354	0.4	1188	54	1200	50	1,206	21	0,4	1205	38

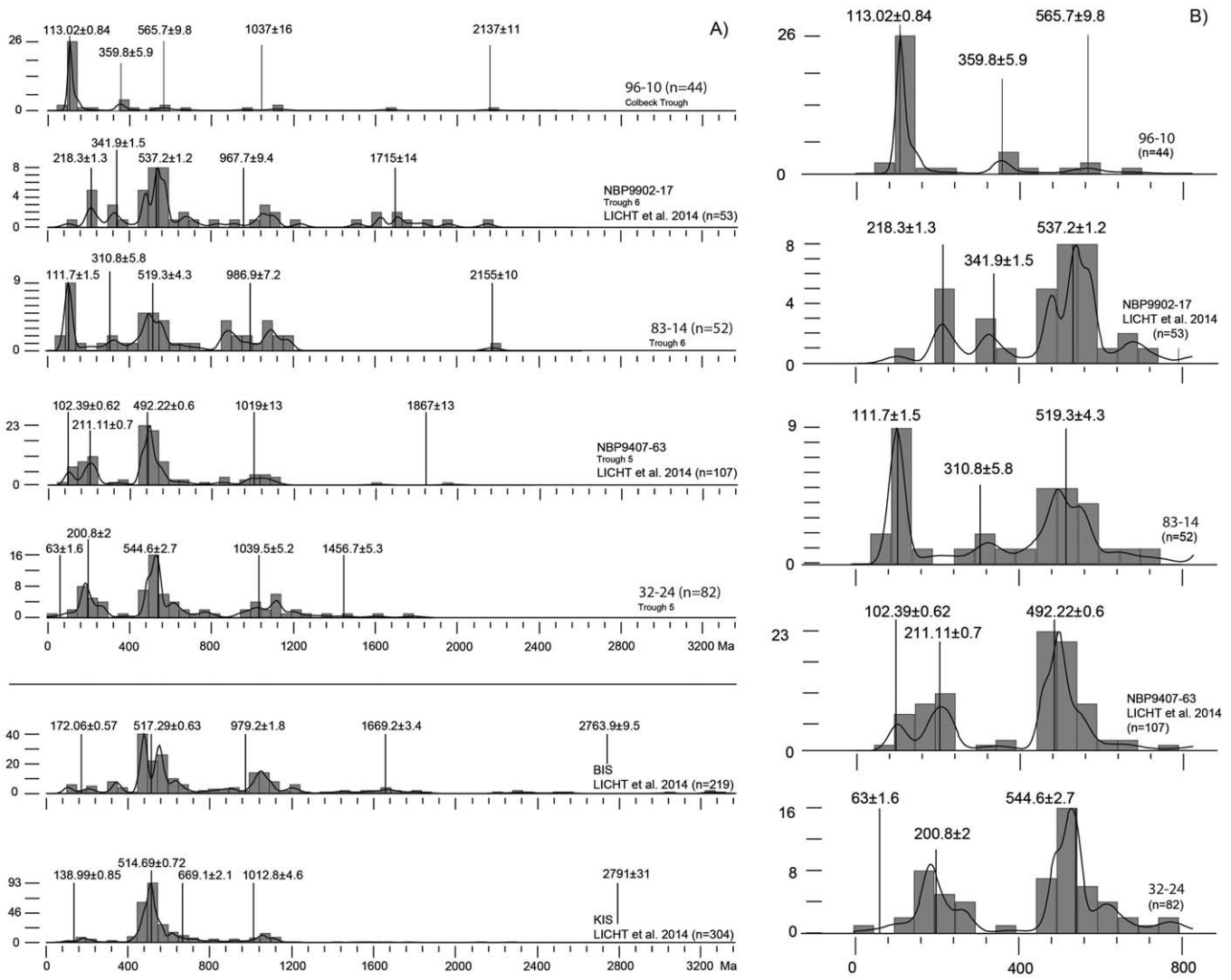

Figure 5. (a) Kernel Density Estimates and histograms for the Zrn-UPb samples, realized with the DensityPlotter software [*Vermeesch*, 2012]. Peaks automatically found by the DensityPlotter software. The results of *Licht et al.* [2014], regarding Ross Sea and Ice Streams samples are also displayed (BIS: Bindschadler Ice Stream; KIS: Kamb Ice Stream); (b) zoom of the 0–800 Ma interval of the Ross Sea samples plots (from this work and *Licht et al.* [2014]).

core were analyzed, no significant variability with depth was observed. Therefore, results obtained from the same core are presented and discussed together.

The easternmost samples from cores located in Sulzberger Bay yield Late Cretaceous to Early Eocene ages.

The Ross Sea samples yield multiple age populations. In order of abundance, these are as follows: Cretaceous to Eocene (p3, p4, p5 in Table 4), Late Triassic-Jurassic (p6 in Table 4), and Oligocene (p2 in Table 4). Age populations represented by less than three crystals are reported in Table 4 (marked by an asterisk) and Figure 6 but are not considered significant for interpretation.

4. Discussion

4.1. Clasts Provenance

Gravel-sized clasts found in LGM and post-LGM intervals from sampled piston cores should reflect the bedrock lithologies of West Antarctica, as suggested by many provenance studies and ice-flow reconstructions [*Licht et al.*, 2005; *Farmer et al.*, 2006; *Licht and Palmer*, 2013; *Licht et al.*, 2014].

Geochemistry, Geophysics, Geosystems

10.1002/2016GC006728

Table 4. AFT Data: Central Ages Calculated Using Dosimeter Glass CN5 and z-CN5 = 344.94 ± 27.24[a]

			Spontaneous		Induced			Dosimeter								
Sample	Depth (cm)	Grains (n)	ρs	Ns	ρi	Ni	P(χ^2)	ρd	Nd	Central Age Ma ± (1σ)	P1 Ma ± (1σ), %	P2 Ma ± (1σ), %	P3 Ma ± (1σ), %	P4 Ma ± (1σ), %	P5 Ma ± (1σ), %	P6 Ma ± (1σ), %
96–11	40–43	40	11.20	2368	23.70	5005	0.3	8.79	2285	72.5 ± 6.3				65.6 ± 5.7, 71.8	92.9 ± 10.0, 28.2	
96–16	2–6	40	10.80	1465	23.60	3200	0.0	8.74	2272	69.7 ± 6.4			54.5 ± 6, 40.8	81.8 ± 8, 59.2		
96–10	9–14; 25–29; 188–190	138	5.82	3174	13.37	6985	0.1	9.86	2563	77.6 ± 2.5		36.2 ± 5.3, 12.9		73.5 ± 7.3, 48.8	93.0 ± 14.6, 21.2	142.8 ± 200, 3.5
32–27	55–60; 105–110	63	9.60	1266	22.15	2920	0.0	9.34	2429	72.9 ± 4.2		21.4 ± 4.7, 8.3	45.8 ± 7.5, 7.3	74.2 ± 7.1, 67.0	115.2 ± 22.0 17.4	
99–17	134–139	35	9.90	978	15.70	1547	0.0	9.16	2382	108.6 ± 13.4		*26.6 ± 7.9, 7.5		68.9 ± 7.5, 29.5		156.4 ± 16.0, 62.9
83–14	81–86; 183–190; 231–236	91	9.58	1880	16.15	4798	1.6	9.83	2556	56.0 ± 3.0		26.9 ± 5.7, 7.5	45.0 ± 5.2, 37.7	74.5 ± 5.2, 42.3	96.0 ± 8.1, 9.5	*156.5 ± 2.9
62–16	111–117; 151–156	80	11.16	3045	16.66	4527	0.0	10.65	2769	111.4 ± 6.4		*29.6 ± 14.5, 2.3		77.9 ± 6.5, 45.4	129.1 ± 10.5,32.1	221.5 ± 16.6, 20.2
94–58	170–173	40	12.00	958	22.30	1781	0.0	8.95	2327	83.2 ± 9.2			44.7 ± 5.7, 26.9		92.7 ± 9.5,61.8	164.8 ± 28.4, 11.4
32–24	416–420	61	14.43	2280	25.93	2677	0.0	9.26	2408	82.5 ± 5.9	*5.8 ± 3.6, 3.2	35.4 ± 5.9, 13.9		74.5 ± 6.9, 47.3	113.0 ± 15.5,14.8	155.5 ± 16.8, 20.8

[a]ρs: spontaneous track densities (105 cm^2) measured in internal mineral surfaces; Ns: total number of spontaneous tracks; ri and rd: induced and dosimeter track densities (106 cm^2) on external mica detectors (g = 0.5); Ni and Nd: total numbers of tracks; P(χ^2): probability of obtaining c^2-value for n degrees of freedom (where n = number of crystals-1); a probability >5% is indicative of an homogenous population. Samples with a probability < 5% have been analyzed with the binomial peak-fitting method to obtain the P1–P4 fitted peaks (P: age population). Peak values signed with * are represented by less than three crystals, and therefore they are considered non significant and not involved in discussion.

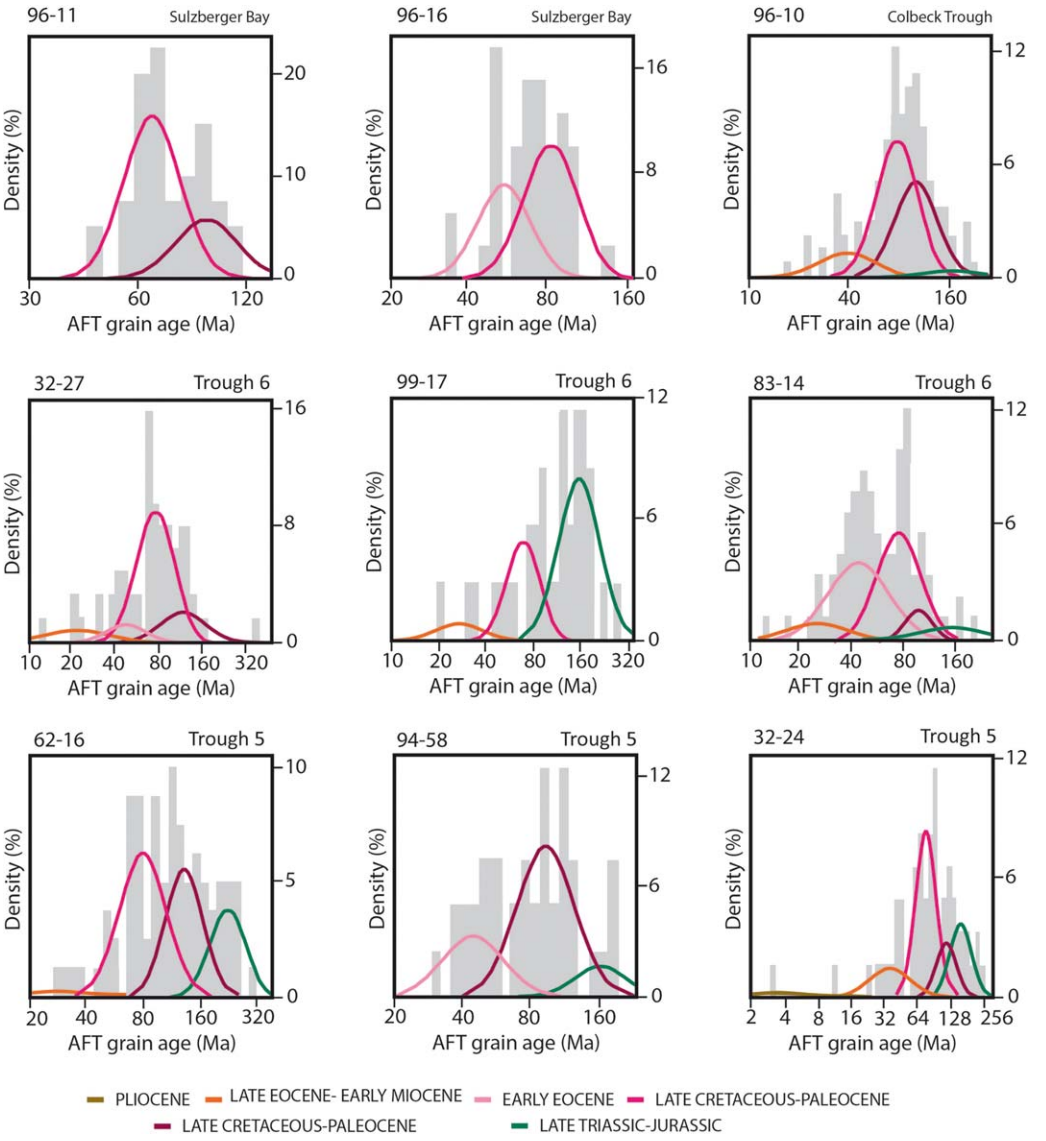

Figure 6. Histogram for AFT ages with best fit peaks, calculated with the Binomfit software [*Brandon*, 1996].

The suite of clasts found in the Eastern Ross Sea cores shows a predominant fraction composed by low-grade metasediments. The only known low-grade metamorphic unit in Marie Byrd Land is the Swanson Formation, a quartz-rich metaflysch sequence that is well exposed in the Swanson, Denfield, McKay, Clark and Allegheny Mountains in western Marie Byrd Land [*Wade et al*., 1977a, 1977b, 1978; *Bradshaw et al*., 1983]. Moreover, correlative metasediments crop out in isolated nunataks, such as La Gorce peak, in Edward VII Peninsula [*Wade et al*., 1977c; *Adams et al*., 1995; *Kleinschmidt and Petschick*, 2003]. Other greenschist facies metasediments crop out in Ruppert and Hobbs Coast [*Pankhurst et al*., 1998, *Brand*, 1979].

Fine to medium grained metasandstones and metagraywackes (i.e., Thin section 6, Figure 3) found in marine cores are similar in texture, grain size and metamorphic grade (sub-greenschist facies paragenesis) to those belonging to the Swanson Formation sequences [*Bradshaw et al*., 1983]. Furthermore, some samples exhibit thermal metamorphism with spotted texture (i.e., Thin section 62, Figure 3), such as some bedrock portions of Swanson Formation rocks which underwent contact metamorphism due to pluton emplacement [*Bradshaw et al*., 1983; *Adams et al*., 1995; *Kleinschmidt and Petschick*, 2003].

White mica analysis carried out on micas defining the cleavage in metasedimentary clasts (Figure 4c) show a variable composition, in most cases with a higher phengitic component (Si = 3.2–3.4 atoms per formula unit), compared to those in Bailey Ridge phyllite from PRR (Si < 3.1 a.p.f.u.) which is attributed to Swanson

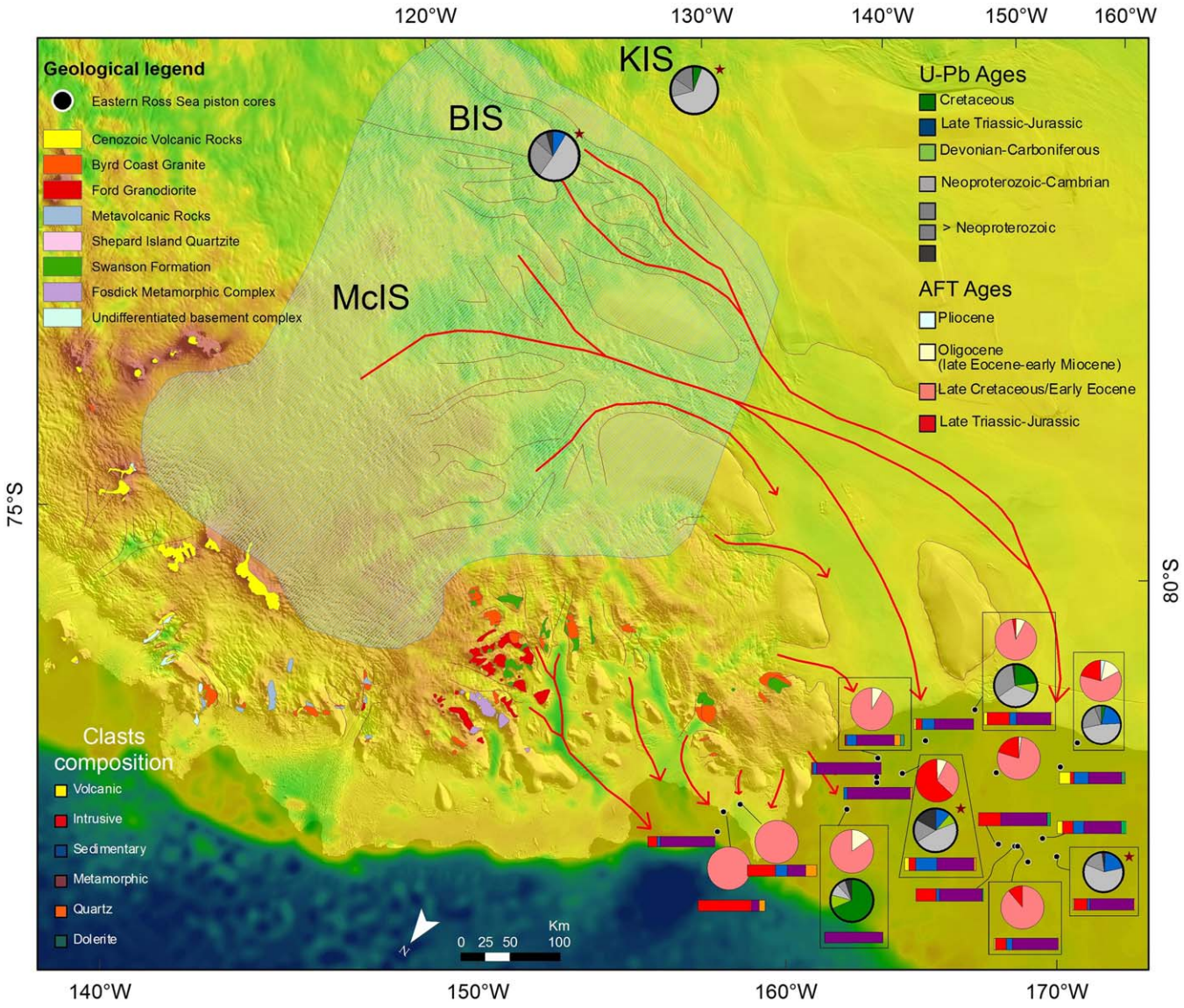

Figure 7. Bedmap of Marie Byrd Land region with geological units and AFT, Zrn-UPb, and clast distribution data. Also ice flow paths reconstruction and LGM inferred catchment area are shown. Horizontal histograms show lithologies distribution, while pie charts evidence AFT and Zrn-UPb ages distributions. Samples marked with a red star are from *Licht et al.* [2014]. McIs: MacAyeal Ice Stream; BIS: Bindschadler Ice Stream; KIS: Kamb Ice Stream. Geologic map from *Wade et al.* [1977a, 1977b, 1977c, 1978].

Formation. This difference could be due to different metamorphic conditions, namely higher pressure (4–8 kbar or higher), in comparison to the low pressure regime suggested by the sample from PRR (~2 kbar following the method described in *Massonne and Schreyer* [1987]). Literature data clearly indicate that no other high pressure and low-grade units are known in the region. However, medium to high pressure conditions are recorded in the Fosdick migmatite-granite complex where a Devonian-Carboniferous event (~820–870°C, 7.5–11.5 kbar) was superimposed by a Cretaceous high-grade overprint at ~830–870°C and ~6–7.5 kbar [*Korhonen et al.*, 2010a, 2010b, 2012]. Therefore, metasedimentary clasts found in the marine record could come from the erosion of rocks belonging to Swanson Formation, or a lithologically similar unit which experienced moderately high P low-grade metamorphism, or to a lower grade correlative of the Fosdick complex, even if white mica is nearly absent from Fosdick and Alexandra migmatite complexes. An alternative source could be indicated in a lithologically similar unit that is younger than Swanson Formation (at least post-Permian) and that has been considered as the (meta)-sedimentary protolith of the metamorphic paragneiss cropping out in Alexandra Mountains, in Edward VII Peninsula [*Pankhurst et al.*, 1998]. However,

the overall mineral data so far available from both clasts and bedrock samples from the Swanson Formation are still few and they do not allow a conclusive and robust statement to demonstrate this interpretation. Even available mineral chemistry data of *Smith* [1996] from Alexandra Mountains refer to higher grade rocks and to different minerals.

The petrographic features of the two groups of granitoids identified in detrital clasts are similar to those of the two granitic suites cropping out in Marie Byrd Land, the Devonian Ford Granodiorite, and the Cretaceous Byrd Coast Granite. The black and white granodioritic to tonalitic biotite-hornblende variety (i.e., Thin section 15 in Figure 3) is similar in texture, grain size and modal mineralogy to those exhibited by granodioritic to tonalitic Ford Granodiorite [*Weaver et al*., 1991, *Yakymchuk et al*., 2015]. Chemical analysis of clinoamphiboles revealed similarities between Mg-hornblendes found in a biotite-hornblende tonalite from marine record and those of a Ford Granodiorite sample from the Phillips Mountains (Figure 4a). Also biotites from these two samples show a similarity in composition (Figure 4b). This calc-alkaline metaluminous to peraluminous I-type suite is widespread in the Ford Ranges and has its easternmost outcrop in Ruppert Coast [*Weaver et al*., 1991; *Pankhurst et al*., 1998]. On the contrary, the pinkish porphyritic monzogranite and leucogranite variety (i.e., Thin section 5 in Figure 3) exhibits similar petrographic features with the alkaline suite of the Byrd Coast Granite. The latter is common in Edward VII Peninsula, the Ford Ranges, and Ruppert Coast [*Weaver et al*., 1991, 1992, 1994; *Adams et al*., 1995], with a predominantly leucogranite and syenogranite suites. Alkaline porphyritic varieties found in marine data set could be associated with the Byrd Coast Granite too, as hypabyssal types of epizonal emplacement.

Sedimentary clasts found in piston cores (mainly quartz-arenite, graywackes, and siltstones) could belong to rocks from Swanson Formation, even if they do not show any metamorphic overprint, or to a unit of sedimentary rocks in the subglacial environment, that is nowhere exposed. In the first case, this would mean the presence in West Antarctica of portions of the Swanson Formation that exhibit no metamorphic overprint. The second case is not directly verifiable, however, an airborne gravity model over Edward VII Peninsula and the Ford Ranges [*Luyendyk et al*., 2003] mapped some low-density subglacial units which could be made up of porphyritic varieties of Byrd Coast Granite, felsic volcanic rocks or sedimentary deposits. Because all of the exposed Swanson Formation in the Ford Ranges, together with its correlatives in northern Victoria Land and New Zealand are metamorphosed [*Adams et al*., 1995], it is difficult to imagine large areas of nonmetamorphic Swanson Formation which could produce a significant marine detrital record. Therefore, our favored interpretation is that detrital sedimentary clasts derive from a subglacial sedimentary unit that is so far undetected in the region. A possibility for the source rock could be portions of unmetamorphosed equivalent of the post-Permian unit in Edward VII Peninsula, considered the protolith of the Alexandra Mountains paragneisses [*Pankhurst et al*., 1998].

Volcanic rocks in Marie Byrd Land are well exposed as Cenozoic eruptive centers in the Flood Range, Hobbs Coast, and Executive Committee Range [*LeMasurier and Rex*, 1989, 1990; *Panter et al*., 1997, 2000; *Hart et al*., 1997]. These volcanoes are composed primarily by felsic alkaline lavas (phonolite, trachyte, and intermediate rocks) that comprise almost all the rocks exposed above ice level in most inland volcanoes as in Flood Range [*LeMasurier et al*., 2011]. Pleistocene basaltic rocks were found also in the Fosdick Mountains [*Gaffney and Siddoway*, 2007]. Volcanic clasts (i.e., Thin section 60), are very rare in the marine data set: they show petrographic characteristics and felsic alkaline modal mineralogy which make them comparable to the Marie Byrd Land volcanic province. It is noteworthy that, although the bedrock geology testifies to the presence of many volcanic centers, volcanic detritus is rare in Eastern Ross Sea. This is in accordance with analysis carried out on detrital coarse sand from Eastern Ross Sea cores by *Anderson et al*. [1992], who identified specific petrographic provinces for Troughs 5 and 6 composed mainly by schists, granites, rounded quartz, and minor amount of gneisses and diabase. Also data relating to subglacial till from Whillans Ice Stream in West Antarctica [*Vogel et al*., 2006] shows a lack of volcanic detritus, even if the catchment area of this ice stream could be related to the Transantarctic Mountains [*Licht et al*., 2014]. One hypothesis which could explain the rarity of volcanic lithologies is that their presence in the marine record among gravel-sized clasts has been diluted by the long transport from known eruptive centers located in Flood Range and Executive Committee Range, or that the clasts are physically weathered. While other lithologies found in the marine record have their correlatives in bedrock geology close to the Marie Byrd Land coast, the volcanic clasts have their closest correlative outcrops in the Fosdick Mountains, requiring a very long transport (and stronger erosion) and a LGM ice flow path different from the modern draining system. The second hypothesis

implies some unexposed volcanic sources beneath the Ice Sheet in the region east of the Ford Ranges; aerogeophysical surveys carried out over the WAIS (in particular the region of Ice Streams C and D, *Behrendt et al*., 1994, 1996, 2004] revealed a series of magnetic and topographic anomalies interpreted to be subglacial volcanic centers: some of them are supposed to be the remnants of residual topography after glacial removal by the WAIS. Also data from *Ferraccioli et al*. [2002] and *Luyendyk et al*. [2003] suggest the presence of sub-ice volcanic centers in western Marie Byrd Land. These combined data suggest the presence of a subglacial source of the detrital clasts found in our data set, rather than a source located farther east in MBL, even if the statistical rarity of clasts in marine record should imply volumetrically minor sources.

Dolerites and other mafic porphyritic varieties found in marine cores could be related to mafic plutonism throughout Marie Byrd Land during Cretaceous crustal extension, with emplacement of numerous dykes, sills and small plutons [*Saito et al*., 2013; *Siddoway et al*., 2005; *Storey et al*., 1999; *Weaver et al*., 1994]. The rock types are widespread from Huppert-Hobbs Coast to Fosdick Mountains and Ford Ranges.

4.2. Data Integration, With Implications for Tectonic and LGM Ice-Flows Reconstructions

In the sample located in Colbeck Trough (96–10) and in Sulzberger Bay (96–11; 96–16) most of the AFT and Zrn-UPb dates are Cretaceous-Eocene, reflecting a local sedimentary provenance from exposed or concealed gneiss domes, or Byrd Coast Granites (or thermally overprinted Swanson Formation) as suggested by *Adams et al*. [1995]. Clasts are predominantly composed of granitoid and metasedimentary lithologies, with an absence of volcanic detritus (Figure 7). New AFT ages accord with the bedrock AFT ages of *Adams et al*. [1995] and *Lisker and Olesch* [1998] on rocks from Edward VII Peninsula. Similar AFT ages are reported for mylonitic gneisses dredged in Colbeck Trough, very close to Edward VII Peninsula [*Siddoway et al*., 2004b], and the Fosdick and Chester Mountains in the Ford Ranges [*Richard et al*., 1994]; therefore, a mixing of local (Edward VII Peninsula) and distal (Ford Ranges) sources cannot be excluded for these cores, in particular for the core 96–11 which is located farther from the coast. Indirect information could account for such mixing: indeed, regional LGM ice-flows pattern from the Ford Ranges to the Sulzberger Bay is supported by the geomorphological study of *Sugden et al*. [2005]. Sample 96–10 from Colbeck Trough shows an AFT Oligocene population, possibly a reflection of Oligocene AFT ages found in Ford Ranges [*Lisker and Olesch*, 1998], but since the position of this core suggests a direct ice draining from Edward VII Peninsula to Colbeck Trough, this implies an Oligocene local exhumation for this region.

Most of the sediments of troughs 5 and 6 (Figure 7) yield Neoproterozoic-Cambrian Zrn-UPb age and Cretaceous AFT ages. Clasts consist mainly of metasedimentary lithologies followed by granitoids and sedimentary clasts (Figure 7). This is compatible with a prevalent Swanson Formation source, associated with rocks affected by Cretaceous extensional tectonism following the Byrd Coast Granite emplacement. The most consistent Zrn-UPb Precambrian age is 987–1039 Ma; this age population appears to be quite common from both sides of the Ross Embayment, being present in detrital zircons from offshore samples located in the Central and Western Ross Sea [*Licht et al*., 2014; *Licht and Palmer*, 2013], and from Beacon Supergroup rocks in the central Transantarctic Mountains [*Elliot and Fanning*, 2008]. However, since this age population is present also from Swanson Formation rocks [*Pankhurst et al*., 1998; *Yakymchuk et al*., 2015] and from BIS and KIS subglacial till samples [*Licht et al*., 2014] (Figure 7), direct attribution to a West Antarctic source for this age population appears to be likely for trough 5 and 6 samples.

However, other minor populations of ages show the existence of exhumed bedrock having different crystallization-cooling paths.

1. Cretaceous and Devonian-Carboniferous Zrn-UPb age populations (cores 96–10; 83–14; 32–24 and 94–63; 99–17; Kamb Ice Stream from *Licht et al*. [2014]) can be associated with Byrd Coast Granite and Ford Granodiorite pluton emplacement or their related migmatites, respectively.
2. A Late Triassic-Jurassic crystallization/metamorphism-cooling event is indicated by both Zrn-UPb and AFT dates (core 99–17 in trough 6 and all the samples in trough 5). The Zrn-UPb Triassic-Jurassic population was already been found from some offshore sites [*Licht et al*., 2014]. A similar population of ages is documented in West Antarctica from Zrn-UPb data of *Riley et al*. [2016] in Thurston Island, where both Triassic and Jurassic magmatism occurred. The former is known also from Kohler Range in Walgreen Coast (eastern Marie Byrd Land) [*Pankhurst et al*., 1998]. The closest known Zrn-UPb ages, although slightly older than our age populations, have been found as minor peak population by *Pankhurst et al*. [1998] from Alexandra Mountains paragneisses, in Edward VII Peninsula. However, as this population is

absent or negligible in offshore samples located close to the Edward VII Peninsula and Roosevelt Island coasts, we suggest that it can be used as a proxy for the contribution of local versus distal sedimentary provenance.

3. An Oligocene AFT age population is present in most of the cores both in troughs 5 and 6; this may correlate to an Oligocene-Pliocene cooling event documented in central Marie Byrd Land, that was related to the Oligocene-Pliocene volcanism and localized uplift (Hobbs Coast) [*Hart et al*., 1997; *LeMasurier and Rex*, 1982]. *Spiegel et al*. [2016] found an early Miocene AFT age population from Hobbs Coast glaciomarine sediment and they interpreted this age population as the result of an enhanced Neogene denudation, implying that uplift and relief formation in eastern Marie Byrd Land also started at about 20 Ma. Our samples record slightly an older age population, except for one sample (32–27 core) that has a similar age peak (P2 in Table 4). This similarity could imply that source rocks which experienced a ∼20 Ma exhumation event and provided detritus to offshore sites in the Eastern Ross Sea are located in a region involved in the uplift of Marie Byrd Land Dome, supporting the hypothesis of *Spiegel et al*. [2016]. However, a volcanic source for apatites yielding this age cannot be excluded, since volcanoes of similar age are present in the central Marie Byrd Land [*LeMasurier and Rex*, 1982].

Trough 6 core sediments are heterogeneous, likely due to mixed local (e.g., core 83–14, located close to Roosevelt Island coasts) and distal sedimentary provenance. This variability is also seen in the clast distribution record, with cores 96–09 and 96–08 characterized almost exclusively by metamorphic clasts, while the other cores in the center of the trough are composed also of granitoids and sedimentary clasts with negligible volcanic rocks. It is probable that the easternmost two cores of trough 6, proximal to Edward VII Peninsula coast, have been influenced by local ice masses flowing from this region. On the contrary, the core sediments of trough 5 yield more homogeneous Zrn-UPb and AFT age populations, suggesting a common provenance, from one or more Ice Streams draining Marie Byrd Land, and possibly yet more distal. This possibility supports the hypothesis of long transport paths, with a major erosion and desegregation of more unstable lithologies such as volcanic ones.

Comparing the Zrn-UPb results to those obtained by *Licht et al*. [2014] for the Bindschadler Ice Stream, it can be noticed that the Cretaceous, Carboniferous and Late Triassic-Jurassic populations are much more prevalent in the Ross Sea sediments (19–45% in the sediments with significant distal provenance) than in the Bindschadler Ice Stream (8.6%). This suggests that the major sedimentary flux into this sector of the Ross Sea at the LGM was from the MacAyeal Ice Stream with a minor contribution of the Bindschadler Ice Stream. So far, no geo and thermochronological data of the MacAyeal Ice Stream are available, but from the present data set and *Licht et al*. [2014] a complex catchment area is expected, well compatible with the Marie Byrd Land geology.

The data presented in this study and by *Licht et al*. [2014] imply that rocks formed or metamorphosed and cooled to low T ($<\sim$100°C) in the Late Triassic-Jurassic are present in the MacAyeal and Bindschadler Ice Streams LGM catchment regions. *Korhonen et al*. [2010a] report few inherited zircon grains of both Triassic and Jurassic ages from Cretaceous granite in the Fosdick Mountains. So far such an event had been documented in western Marie Byrd Land as inherited zircon grains from Alexandra Mountains paragneisses [*Pankhurst et al*., 1998].

The finding that most of the AFT dates are Cretaceous to Eocene suggest that a regional exhumation may have occurred at the time of the Byrd Coast Granite emplacement and following this event in the source region. Heating preceding this exhumation episode may have reset AFT dates, with respect to previous cooling events (Figure 8). However, Late Triassic-Jurassic dates were not reset, implying that the portion of the catchment to which they belong was not affected by Cretaceous exhumation.

To conclude we infer a local provenance for samples located in the Sulzberger Bay and very close to the coastlines of Edward VII Peninsula and Roosevelt Island, a mixed local and distal provenance for samples located in trough 6, and mainly a distal provenance for samples located in trough 5. For both the troughs we hypothesize a possible subglacial unit that was eroded to provide for significant amount of sedimentary clasts.

Most of the distal sediments were discharged by the MacAyeal Ice Stream and the Bindschadler Ice Streams, the drainage area of the former being fully compatible with the Marie Byrd Land geology. However, Late

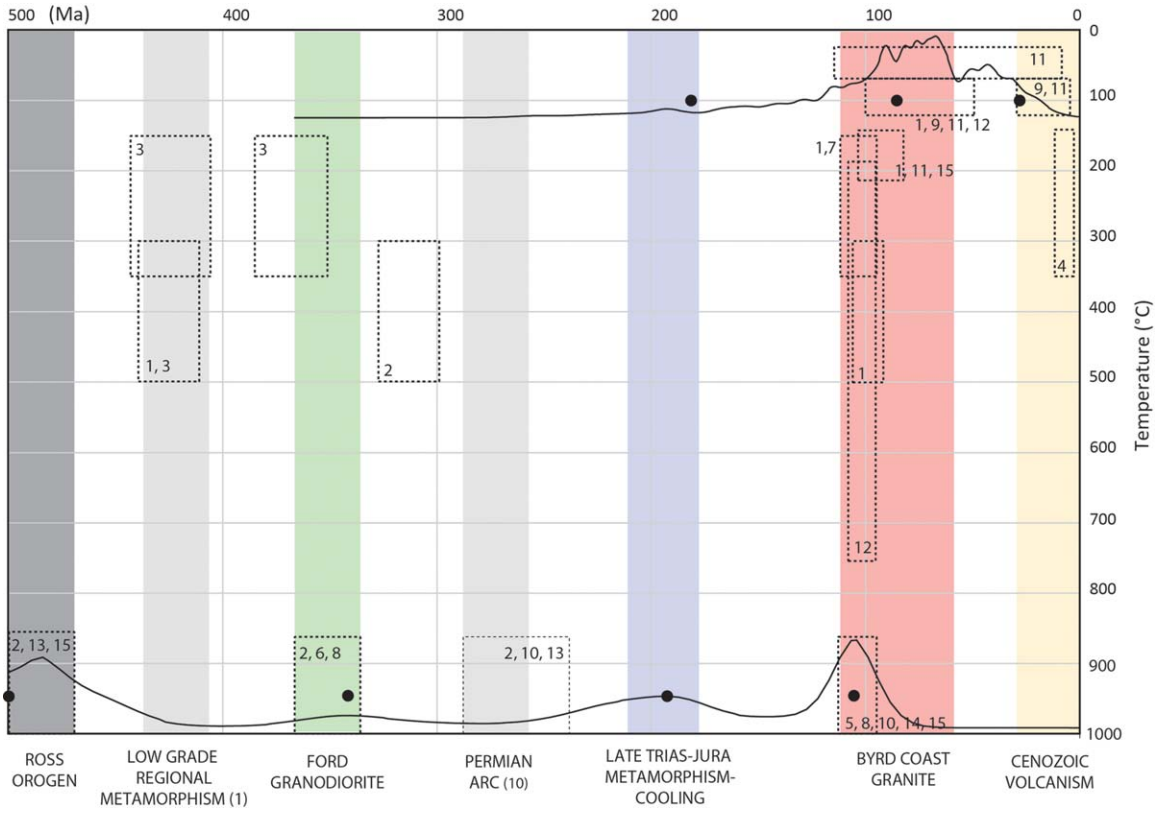

Figure 8. Summary of the geochronology and thermochronology of the Marie Byrd Land (dashed boxes, from literature), and of the Ross Sea sediments (black lines represent the Kernel Density Estimate curves of Zrn-UPb and AFT dates, black dots indicate the major population ages). 1: *Adams et al.* [1995]; 2: *Pankhurst et al.* [1998]; 3: *Adams* [1986]; 4: *Hart et al.* [1997]; 5: *Saito et al.* [2013]; 6: *Siddoway and Fanning* [2009]; 7: *Siddoway et al.* [2005]; 8: *Brown et al.* [2016]; 9: *Lisker and Olesch* [1998]; 10: *Mukasa and Dalziel* [2000]; 11: *Spiegel et al.* [2016]; 12: *Richard et al.* [1994]; 13: *Yakymchuk et al.* [2015]; 14: *McFadden et al.* [2010a, 2010b]; 15: *Contreras et al.* [2012]. Vertical bands indicate the major geological events detected by geochronology and thermochronology (from literature and from present work).

Triassic-Jurassic dates, already inferred by *Licht et al.* [2014], and with few evidences in the Marie Byrd Land outcrops, were found to constitute a significant component of the Ross Sea sediments Zrn-UPb and AFT.

5. Conclusions

In this study, a multianalytical provenance analysis involving three different techniques was carried out to LGM glaciomarine sediments located in the Eastern Ross Sea and in Sulzberger Bay. The new detrital data inform about the WAIS dynamics and the features of the eroded area. The main conclusions are summarized as follows:

1. Gravel-sized clasts petrographic analysis revealed a source area defined mainly by low-grade-metasedimentary units, namely Swanson Formation in western Marie Byrd Land and its correlatives in the region.
2. Devonian-Carboniferous and Cretaceous Zrn-UPb age populations signify sources in the Ford Granodiorite and Byrd Coast Granite (or their related migmatites complexes) as the main sources for granitoid detritus, pointing out a source region compatible with western Marie Byrd Land geology.
3. The rarity of both volcanic detritus and volcanic-related age populations suggests a volumetrically minor source located somewhere in a subglacial environment beneath WAIS, pyroclastic ejecta, or a distal source in volcanic ranges in central Marie Byrd Land. The latter requires a longer transport distance and major erosion. Unexposed sedimentary units are supposed to exist beneath WAIS in the LGM catchment areas that could provide detrital clasts to the sedimentary record in the Eastern Ross Sea.
4. Significant detrital Zrn-UPb and AFT Triassic-Jurassic age populations, already documented in detrital studies of the region, suggests the presence of quite widespread rocks that either formed or metamorphosed at that time in the LGM catchment areas. These rocks are presently not exposed in western Marie Byrd Land, but rocks of similar ages are found in Thurston Island and Walgreen Coast (eastern Marie Byrd Land).

5. The source area for the sediments is considered to be Edward VII Peninsula for the samples located in Sulzberger Bay and in Colbeck Trough, and the catchment areas of MacAyeal and to a lesser extent Bindschadler Ice Stream for samples located in troughs 5 and 6. These draining patterns for the LGM are coherent with the composition and ages of detrital sediments, with the inland subglacial region of western Marie Byrd Land being the main source area.
6. Detrital AFT ages found in Eastern Ross Sea sediments inform about an Oligocene exhumation event occurred both in local source region (Edward VII Peninsula) and in distal source area. This event could be related to extensional tectonic setting [*Siddoway*, 2008] of this shoulder of the West Antarctic Rift System.

Acknowledgments
This work was funded by PNRA 2013/AZ2.08 project. All data used to support this study are present in the paper, in references, and in the supporting information in form of tables. We thank the staff of the Marine Geology Antarctic Research Facility of Tallahassee, Florida (USA) for their support in the stage of core selection and logging and for providing the samples of this study. We also thank Anne Grunow at the Polar Rock Repository in the Byrd Polar Research Centre, Ohio State University, for providing useful samples of rocks from the study area. Mineral chemistry full data and Zrn-UPb data are available as supporting information. We are grateful to two anonymous reviewers for their precious comments and advices that helped improve the earlier version of this paper.

References

Adams, C. J. (1986), Geochronological studies of the Swanson Formation of Marie Byrd Land, West Antarctica, and correlation with northern Victoria Land, East Antarctica, and South Island, New Zealand, *N. Z. J. Geol. Geophys.*, *29*, 345–358, doi:10.1080/00288306.1986.10422157.

Adams, C. J., D. Seward, and S. D. Weaver (1995), Geochronology of Cretaceous granites and metasedimentary basement on Edward VII Peninsula, Marie Byrd Land, West Antarctica. *Antarct. Sci.*, *7*, 265–276, doi:10.1017/S095410209500037X.

Adams, C. J., N. Mortimer, H. J. Campbell, and W. L. Griffin (2013), The mid-Cretaceous transition from basement to cover within sedimentary rocks in eastern New Zealand; evidence from detrital zircon age patterns, *Geol. Mag.*, *150*, 455–478, doi:10.1017/S0016756812000611.

Anderson, J., S. Shipp, L. Bartek, and D. E. Reid (1992), Evidence for a grounded ice sheet on the Ross Sea continental shelf during the late Pleistocene and preliminary paleodrainage reconstruction, *AGU Antarct. Res. Ser.*, *57*, 39–62, doi:10.1029/AR057p0039.

Anderson, J. B., et al. (2014), Ross Sea paleo-ice sheet drainage and deglacial history during and since the LGM, *Quat. Sci. Rev.*, *100*, 31–54, doi:10.1016/j.quascirev.2013.08.020.

Anderson, J. B., C. F. Brake, and N. C. Myers (1983), Sedimentation in the Ross Sea, Antarctica, *Mar. Geol.*, *57*, 295–333, doi:10.1016/0025-3227(84)90203-2.

Barker, P. F., and A. Camerlenghi (2002), Glacial history of the Antarctic Peninsula from Pacific Margin Sediments, in *Proceedings of the Ocean Drilling Program, Scientific Results*, vol. 178, 1–40, edited by P. F. Barker et al., Ocean Drill. Program, College Station, Tex.

Behrendt, J. C., D. D. Blankenship, C. A. Finn, R. E. Bell, R. E. Sweeney, S. M. Hodge, and J. M. Brozena (1994), Casertz aeromagnetic data reveal Late Cenozoic flood basalts (?) in the West Antarctic Rift System, *Geology*, *22*, 527–530.

Behrendt, J. C., R. Saltus, D. Damaske, A. McCafferty, C. A. Finn, D. Blankenship, and R. E. Bell (1996), Patterns of late Cenozoic volcanic and tectonic activity in the West Antarctic Rift System revealed by aeromagnetic surveys, *Tectonics*, *15*, 660–676.

Behrendt, J. C., D. D. Blankenship, D. L. Morse, and R. E. Bell (2004), Shallow source aeromagnetic anomalies observed over the West Antarctic Ice Sheet compared with coincident bed topography from radar ice sounding: New evidence for glacial "removal" of subglacially erupted Late Cenozoic rift related volcanic edifices, *Global Planet. Change*, *42*, 177–193.

Bradshaw, J. D., P. B. Andrews, and B. D. Field (1983), Swanson formation and related rocks of Marie Byrd Land and a comparison with the Robertson Bay Group of northern Victoria Land, *Antarct. Earth Sci.*, *1982*, 274–279.

Brand, J. F. (1979), Low Grade Metamorphic Rocks of the Ruppert and Hobbs Coasts of Marie Byrd Land, Antarctica, MSc thesis, 49 pp., Tex. Tech Univ., Lubbock, Tex.

Brandon, M. T. (1996), Probability density plot for fission-track grain-age samples, *Radiat. Meas.*, *26*(5), 663–676, doi:10.1016/S1350-4487(97)82880-6.

Brown, C. R., C. Yakymchuk, M. Brown, C. M. Fanning, F. J. Korhonen, P. M. Piccoli, and C. S. Siddoway (2016), From source to sink: Petrogenesis of Cretaceous Anatectic Granites from the Fosdick Migmatite–Granite Complex, West Antarctica, *J. Petrol.*, *57*(7), 1241–1278, doi:10.1093/petrology/egw039.

Contreras, A., C. S. Siddoway, P. Reiners, and G. Gehrels (2012), New insights on the timing and extent of Cretaceous exhumation in the West Antarctic Rift System, from U-Pb and (U-Th)/He zircon analysis, *Geol. Soc. Am. Abstr. Program*, *43*(5), 100.

Di Venere, V. J., D. V. Kent, and I. W. D. Dalziel (1994), Mid-Cretaceous paleomagnetic results from Marie Byrd Land, West Antarctica; a test of post-100 Ma relative motion between East and West Antarctica, *J. Geophys. Res.*, *99*, 15,115–15,139, doi:10.1029/94JB00807.

Domack, E. W., E. A. Jacobson, S. Shipp, and J. B. Anderson (1999), Late Pleistocene–Holocene retreat of the West Antarctic Ice-Sheet system in the Ross Sea: Part 2—Sedimentologic and stratigraphic signature, *Geol. Soc. Am. Bull.*, *111*, 1517–1536, doi:10.1130/0016-7606(1999)111 < 1517:LPHROT>2.3.CO;2.

Droop, G. T. R. (1987), A general equation for estimating Fe^{3+} concentrations in ferromagnesian silicates and oxides from microprobe analyses, using stoichiometric criteria, *Mineral. Mag.*, *51*, 431–435, doi:10.1180/minmag.1987.051.361.10.

Elliot, D. H., and C. M. Fanning (2008), Detrital zircons from upper Permian and lower Triassic Victoria Group sandstones, Shackleton Glacier region, Antarctica: Evidence for multiple sources along the Gondwana plate margin, *Gondwana Res.*, *13*, 259–274.

Farmer, G. L., K. Licht, R. J. Swope, and J. Andrews (2006), Isotopic constraints on the provenance of fine-grained sediment in LGM tills from the Ross Embayment, Antarctica, *Earth Planet. Sc. Lett.*, *249*(1), 90–107, doi:10.1016/j.epsl.2006.06.044.

Ferraccioli, F., E. Bozzo, and D. Damaske (2002), Aeromagnetic signatures over western Marie Byrd Land provide insight into magmatic arc basement, mafic magmatism and structure of the Eastern Ross Sea Rift flank, *Tectonophysics*, *347*, 139–165, doi:10.1016/S0040-1951(01)00242-6.

Gaffney, A. M., and C. S. Siddoway (2007), Heterogeneous sources for Pleistocene lavas of Marie Byrd Land, Antarctica: New data from the SW Pacific diffuse alkaline magmatic province (extended abstract), in *Antarctica: A Keystone in a Changing World. Proceedings and Conference Abstracts*, edited by A. Cooper and C. Raymond, *U.S. Geol. Surv. Open File Rep.*, *2007–1047-ea063*, 4 pp.

Hart, S. R., J. Blusztajn, W. E. LeMasurier, and D. C. Rex (1997), Hobbs Coast Cenozoic volcanism: Implications for the West Antarctic Rift System, *Chem. Geol.*, *139*(1), 223–248, doi:10.1016/S0009-2541(97)00037-5.

Hiess, J., D. J. Condon, N. McLean, and S. R. Noble (2012), $^{238}U/^{235}U$ systematics in terrestrial uranium-bearing minerals, *Science*, *335*(6076), 1610–1614, doi:10.1126/science.1215507.

Horn, I., R. L. Rudnick, and W. F. McDonough (2000), Precise elemental and isotope ratio determination by simultaneous solution nebulization and laser ablation-ICP-MS: Application to U–Pb geochronology, *Chem. Geol.*, *164*(3), 281–301, doi:10.1016/S0009-2541(99)00168-0.

Horstwood, M. S., G. L. Foster, R. R. Parrish, S. R. Noble, and G. M. Nowell (2003), Common-Pb corrected in situ U–Pb accessory mineral geochronology by LA-MC-ICP-MS, *J. Anal. Atom. Spectrom.*, *18*(8), 837–846, doi:10.1039/B304365G.

Hughes, T. (1973), Is the West Antarctic Ice Sheet disintegrating?, *J. Geophys. Res.*, *78*, 7884–7910, doi:10.1029/JC078i033p07884.

Hurford, A. J. (1990), Standardization of fission track dating calibration: recommendation by the Fission Track Working Group of the IUGS Subcommission on Geochronology, *Chem. Geol.*, *80*(2), 171–178, doi:10.1016/0168-9622(90)90025-8.
Hurford, A. J., and P. F. Green (1983), The zeta age calibration of fission-track dating, *Chem. Geol.*, *41*, 285–317.
Ireland, T. R., T. Floettmann, C. M. Fanning, G. M. Gibson, and W. V. Preiss (1998), Development of the early Paleozoic Pacific margin of Gondwana from detrital zircon ages across the Delamerian orogen, *Geology*, *26*, 243–246, doi:10.1130/0091-7613(1998)026 < 0243: DOTEPP>2.3.CO;2.
Ivany, L. C., S. Van Simaeys, E. W. Domack, and S. D. Samson (2006), Evidence for an earliest Oligocene ice sheet on the Antarctic Peninsula, *Geology*, *34*, 377–380.
Jackson, S. E., N. J. Pearson, W. L. Griffin, and E. A. Belousova (2004), The application of laser ablation-inductively coupled plasma-mass spectrometry to in situ U–Pb zircon geochronology, *Chem. Geol.*, *211*(1), 47–69, doi:10.1016/j.chemgeo.2004.06.017.
Ketchum, J. W., S. E. Jackson, N. G. Culshaw, and S. M. Barr (2001), Depositional and tectonic setting of the Paleoproterozoic Lower Aillik Group, Makkovik Province, Canada: Evolution of a passive margin-foredeep sequence based on petrochemistry and U–Pb (TIMS and LAM-ICP-MS) geochronology, *Precambrian Res.*, *105*(2), 331–356, doi:10.1016/S0301-9268(00)00118-2.
Kleinschmidt, G., and R. Petschick (2003), Regional metamorphism of the Swanson Formation, western Marie Byrd Land, Antarctica, *Geol. Jahrb., B95*, 11–33.
Kretz, R. (1983), Symbols for rock forming minerals, *Am. Mineral.*, *68*, 277–279.
Korhonen, F. J., S. Saito, M. Brown, C. S. Siddoway, and J. M. D. Day (2010a), Multiple generations of granite in the Fosdick Mountains, Marie Byrd Land, West Antarctica; implications for polyphase intracrustal differentiation in a continental margin setting, *J. Petrol.*, *51*, 627–670, doi:10.1093/petrology/egp093.
Korhonen, F. J., S. Saito, M. Brown, and C. S. Siddoway (2010b), Modeling multiple melt loss events in the evolution of an active continental margin, *Lithos*, *116*, 230–248, doi:10.1016/j.lithos.2009.09.004.
Korhonen, F. J., M. Brown, M. Grove, C. S. Siddoway, E. F. Baxter, and J. D. Inglis (2012), Separating metamorphic events in the Fosdick migmatite-granite complex, West Antarctica, *J. Metamorph. Geol.*, *30*, 165–192, doi:10.1111/j.1525-1314.2011.00961.x.
Langone, A., A. Caggianelli, V. Festa, and G. Prosser (2014), Time constraints on the building of the Serre Batholith: Consequences for the thermal evolution of the Hercynian continental crust exposed in Calabria (southern Italy), *J. Geol.*, *122*(2), 183–199, doi:10.1086/675227.
Leake, B. E., et al. (1997), Nomenclature of amphiboles: Report of the subcommittee on amphiboles of the International Mineralogical Association, commission on new minerals and mineral names, *Am. Mineral.*, *82*, 1019–1037, doi:10.1180/minmag.1997.061.405.13.
LeMasurier, W. E., and D. C. Rex (1982), Volcanic record of Cenozoic glacial history in Marie Byrd Land and western Ellsworth Land: Revised chronology and evaluation of tectonic factors, *Antarct. Geosci.*, *89*, 725–734.
LeMasurier, W. E., and D. C. Rex (1989), Evolution of linear volcanic ranges in Marie Byrd Land, West Antarctica, *J. Geophys. Res.*, *94*, 7223–7236, doi:10.1029/JB094iB06p07223.
LeMasurier, W. E., and D. C. Rex (1990), Late Cenozoic volcanism on the Antarctic Plate: An overview, in *Volcanoes of the Antarctic Plate and Southern Oceans, Antarct. Res. Ser.*, vol. 48, edited by W. E. LeMasurier and J. W. Thompson, pp. 1–17, AGU, Washington, D. C.
LeMasurier, W. E., S. H. Choi, Y. Kawachi, S. B. Mukasa, and N. W. Rogers (2011), Evolution of pantellerite-trachyte-phonolite volcanoes by fractional crystallization of basanite magma in a continental rift setting, Marie Byrd Land, Antarctica, *Contrib. Mineral. Petrol.*, *162*, 1175–1199, doi:10.1007/s00410-011-0646-z.
Licht, K. J., and J. T. Andrews (2002), The ^{14}C record of Late Pleistocene ice advance and retreat in the Central Ross Sea, Antarctica, *Arct. Antarct. Alp. Res.*, *34*, 324, doi:10.2307/1552491.
Licht, K. J., and E. F. Palmer (2013), Erosion and transport by Byrd Glacier, Antarctica during the Last Glacial Maximum, *Quat. Sci. Rev.*, *62*, 32–48, doi:10.1016/j.quascirev.2012.11.017.
Licht, K. J., N. W. Dunbar, J. T. Andrews, and A. E. Jennings (1999), Distinguishing subglacial till and glacial marine diamictons in the western Ross Sea, Antarctica: Implications for a last glacial maximum grounding line, *Geol. Soc. Am. Bull.*, *111*, 91–103, doi:10.1130/0016-7606(1999)111 < 0091:DSTAGM>2.3.CO;2.
Licht, K. J., J. R. Lederer, and R. Jeffrey Swope (2005), Provenance of LGM glacial till (sand fraction) across the Ross embayment, Antarctica, *Quat. Sci. Rev.*, *24*, 1499–1520, doi:10.1016/j.quascirev.2004.10.017.
Licht, K. J., A. J. Hennessy, and B. M. Welke (2014), The U-Pb detrital zircon signature of West Antarctic ice stream tills in the Ross embayment, with implications for Last Glacial Maximum ice flow reconstructions, *Antarct. Sci.*, *26*, 687–697, doi:10.1017/S0954102014000315.
Lisker, F., and M. Olesch (1998), Cooling and denudation history of western Marie Byrd Land, Antarctica, based on apatite fission-tracks, in *Advances in Fission-Track Geochronology*, pp. 225–240, Springer, Dordrecht, Netherlands.
Ludwig, K. R. (2003), *User's Manual for Isoplot 3.00: A Geochronological Toolkit for Microsoft Excel (No. 4)*, Kenneth R. Ludwig, Berkeley Geochronology Center, Spec. Publ. No. 4.
Luyendyk, B. P., D. S. Wilson, and C. S. Siddoway (2003), Eastern margin of the Ross Sea Rift in western Marie Byrd Land, Antarctica: Crustal structure and tectonic development, *Geochem. Geophys. Geosyst.*, *4*(10), 1090, doi:10.1029/2002GC000462.
Massonne, H.-J., and W. Schreyer (1987), Phengite geobarometry based on the limiting assemblage with K-feldspar, phlogopite, and quartz, *Contrib. Mineral. Petrol.*, *96*, 212–224, doi:10.1007/BF00375235.
McFadden, R. R., C. S. Siddoway, C. Teyssier, and C. M. Fanning (2010a), Cretaceous oblique extensional deformation and magma accumulation in the Fosdick Mountains migmatite-cored gneiss dome, West Antarctica, *Tectonics*, *29*, TC4022, doi:10.1029/2009TC002492.
McFadden, R. R., C. Teyssier, C. S. Siddoway, D. L. Whitney, and C. M. Fanning (2010b), Oblique dilation, melt transfer, and gneiss dome emplacement, *Geology*, *38*, 375–378.
Mosola, A. B., and J. B. Anderson (2006), Expansion and rapid retreat of the West Antarctic Ice Sheet in eastern Ross Sea: Possible consequence of over-extended ice streams?, *Quat. Sci. Rev.*, *25*, 2177–2196, doi:10.1016/j.quascirev.2005.12.013.
Mukasa, S. B., and I. W. D. Dalziel (2000), Marie Byrd Land, West Antarctica: Evolution of Gondwana's Pacific margin constrained by zircon U-Pb geochronology and feldspar common-Pb isotopic compositions, *Geol. Soc. Am. Bull.*, *112*, 611–627, doi:10.1130/0016-7606(2000)112 < 611:MBLWAE>2.0.CO;2.
Naish, T., et al. (2009), Obliquity-paced Pliocene West Antarctic Ice Sheet oscillations, *Nature*, *458*, 322–328, doi:10.1038/nature07867.
Pankhurst, R. J., S. D. Weaver, J. D. Bradshaw, B. C. Storey, and T. R. Ireland (1998), Geochronology and geochemistry of pre-Jurassic superterranes in Marie Byrd Land, Antarctica, *J. Geophys. Res.*, *103*, 2529–2547, doi:10.1029/97JB02605.
Panter, K. S., P. R. Kyle, and J. L. Smellie (1997), Petrogenesis of a phonolite–trachyte succession at Mount Sidley, Marie Byrd Land, Antarctica, *J. Petrol.*, *38*, 1225–1253, doi:10.1093/petroj/38.9.1225.
Panter, K. S., S. R. Hart, P. Kyle, J. Blusztanjn, and T. Wilch (2000), Geochemistry of Late Cenozoic basalts from the Crary Mountains: Characterization of mantle sources in Marie Byrd Land, Antarctica, *Chem. Geol.*, *165*, 215–241, doi:10.1016/S0009-2541(99)00171-0.

Paquette, J. L., and M. Tiepolo (2007), High resolution (5 μm) U–Th–Pb isotope dating of monazite with excimer laser ablation (ELA)-ICPMS, *Chem. Geol.*, *240*(3), 222–237, doi:10.1016/j.chemgeo.2007.02.014.

Pollard, D., and R. M. DeConto (2009), Modelling West Antarctic Ice Sheet growth and collapse through the past five million years, *Nature*, *458*, 329–332, doi:10.1038/nature07809.

Richard, S. M., C. H. Smith, D. L. Kimbrough, P. G. Fitzgerald, B. P. Luyendyk, and M. O. McWilliams (1994), Cooling history of the northern Ford Ranges, Marie Byrd Land, West Antarctica, *Tectonics*, *13*, 837–857.

Riley, T. R., M. J. Flowerdew, R. J. Pankhurst, P. T. Leat, I. L. Millar, C. M. Fanning, and M. J. Whitehouse (2016), A revised geochronology of Thurston Island, West Antarctica, and correlations along the proto-Pacific margin of Gondwana, *Antarct. Sci.*, *29*, 47–60, doi:10.1017/S0954102016000341.

Rocchi, S., W. LeMasurier, and G. Di Vicenzo (2006), Oligocene to Holocene erosion and glacial history in Marie Byrd Land, West Antarctica, inferred from exhumation of the Dorrel rock intrusive complex and from volcano morphologies, *Geol. Soc. Am. Bull.*, *118*, 991–1005.

Saito, S., M. Brown, F. J. Korhonen, R. R. McFadden, and C. S. Siddoway (2013), Petrogenesis of Cretaceous mafic intrusive rocks, Fosdick Mountains, West Antarctica: Melting of the sub-continental arc mantle along the Gondwana margin, *Gondwana Res.*, *23*, 1567–1580, doi:10.1016/j.gr.2012.08.002.

Shipp, S., J. Anderson, and E. Domack (1999), Late Pleistocene–Holocene retreat of the West Antarctic Ice-Sheet system in the Ross Sea: Part 1—geophysical results, *Geol. Soc. Am. Bull.*, *111*, 1486–1516, doi:10.1130/0016-7606(1999)111 < 1486:LPHROT>2.3.CO;2.

Siddoway, C. (2008), Tectonics of the West Antarctic Rift System: New light on the history and dynamics of distributed intracontinental extension, in *Antarctica: A Keystone in a Changing World, Proceedings of the 10th International Symposium on Antarctic Earth Sciences*, edited by A. K. Cooper et al., pp. 91–114, The Natl. Acad. Press, Washington, D. C.

Siddoway, C. S., and C. M. Fanning (2009), Paleozoic tectonism on the East Gondwana margin: Evidence from SHRIMP U–Pb zircon geochronology of a migmatite–granite complex in West Antarctica, *Tectonophysics*, *477*, 262–277, doi:10.1016/j.tecto.2009.04.021.

Siddoway, C. S., S. M. Richard, C. M. Fanning, and B. P. Luyendyk (2004a), Origin and emplacement of a Middle Cretaceous gneiss dome, Fosdick Mountains, West Antarctica, in *Gneiss Domes in Orogeny*, edited by D. L. Whitney, C. Teyssier, and C. S. Siddoway, *Geol. Soc. Am. Spec. Pap.*, *380*, 267–294.

Siddoway, C. S., S. L. Baldwin, P. G. Fitzgerald, C. M. Fanning, and B. P. Luyendyk (2004b), Ross Sea mylonites and the timing of intracontinental extension within the West Antarctic Rift System, *Geology*, *32*, 57–60.

Siddoway, C. S., L. C. Sass III, and R. P. Esser (2005), Kinematic history of the Marie Byrd Land terrane, West Antarctica: Direct evidence from Cretaceous mafic dykes, in *Terrane Processes at the Margin of Gondwana*, edited A. Vaughan, P. Leat, and R. J. Pankhurst, *Geol. Soc. London, Special Pub.*, *246*, pp. 417–438.

Smith, C. H. (1996), Migmatites of the Alexandra Mountains, West Antarctica: Pressure-temperature conditions of formation and regional context, *Geol. Jahrb.*, *B52*, 169–178.

Spiegel, C., J. Lindow, P. J. J. Kamp, and K. Gohl (2016), Tectonomorphic evolution of Marie Byrd Land—Implications for Cenozoic rifting activity and onset of West Antarctic glaciation, *Global Planet. Change*, *145*, 98–115, doi:10.1016/j.gloplacha.2016.08.013.

Storey, B. C., P. T. Leat, S. D. Weaver, J. D. Pankhurst, and S. Kelley (1999), Mantle plumes and Antarctic-New Zealand rifting: Evidence from mid-Cretaceous mafic dykes, *J. Geol. Soc.*, *156*, 659–671, doi:10.1144/gsjgs.156.4.0659.

Storti, F., M. L. Balestrieri, F. Balsamo, and F. Rossetti (2008), Structural and thermochronological constraints to the evolution of the West Antarctic Rift System in central Victoria Land, *Tectonics*, *27*, TC4012, doi:10.1029/2006TC002066.

Sugden, D. E., G. A. Balco, S. G. Cowdery, J. O. Stone, and L. C. Sass (2005), Selective glacial erosion and weathering zones in the coastal mountains of Marie Byrd Land, Antarctica, *Geomorphology*, *67*, 317–334.

Talarico, F. M., and S. Sandroni (2011), Early Miocene basement clasts in ANDRILL AND-2A core and their implications for paleoenvironmental changes in the McMurdo Sound region (western Ross Sea, Antarctica), *Global Planet. Change*, *78*, 23–35, doi:10.1016/j.gloplacha.2011.05.002.

Tiepolo, M. (2003), In situ Pb geochronology of zircon with laser ablation–inductively coupled plasma–sector field mass spectrometry, *Chem. Geol.*, *199*(1), 159–177, doi:10.1016/S0009-2541(03)00083-4.

Tulloch, A. J., J. Ramezani, D. L. Kimbrough, K. Faure, and A. H. Allibone (2009), U-Pb geochronology of mid-Paleozoic plutonism in western New Zealand; implications for S-type granite generation and growth of the east Gondwana margin, *Geol. Soc. Am. Bull.*, *121*, 1236–1261, doi:10.1130/B26272.1.

Van Achterbergh, E., C. G. Ryan, S. E. Jackson, and W. L. Griffin (2001), Data reduction software for LA-ICP-MS. Laser-Ablation-ICPMS in the earth sciences—Principles and applications, *Miner. Assoc. Can.*, *29*, 239–243.

Vermeesch, P. (2012), On the visualisation of detrital age distributions, *Chem. Geol.*, *312*, 190–194, doi:10.1016/j.chemgeo.2012.04.021.

Vogel, S. W., S. Tulaczyk, S. Carter, P. Renne, B. Turrin, and A. Grunow (2006), Geologic constraints on the existence, distribution of West Antarctic subglacial volcanism, *Geophys. Res. Lett.*, *33*, L23501, doi:10.1029/2006GL027344.

Wade, F. A., C. A. Cathey, and J. B. Oldham (1977a), *Reconnaissance Geologic Map of the Guest Peninsula Quadrangle, Marie Byrd Land, Antarctica, Map A-7*, U.S. Antarc. Res. Program, Reston, Va.

Wade, F. A., C. A. Cathey, and J. B. Oldham (1977b), *Reconnaissance Geologic Map of the Boyd Glacier Quadrangle, Marie Byrd Land, Antarctica, Map A-6*, U.S. Antarc. Res. Program, Reston, Va.

Wade, F. A., C. A. Cathey, and J. B. Oldham (1977c), *Reconnaissance Geologic Map of the Alexandra Mountains Quadrangle, Marie Byrd Land, Antarctica, Map A-5*, U.S. Antarc. Res. Program, Reston, Va.

Wade, F. A., C. A. Cathey, and J. B. Oldham (1978), *Reconnaissance Geologic Map of the Gutenko Nunataks Quadrangle, Marie Byrd Land, Antarctica, Map A-11*, U.S. Antarc. Res. Program, Reston, Va.

Weaver, S. D., J. D. Bradshaw, and C. J. Adams (1991), Granitoids of the Ford Ranges, Marie Byrd Land, Antarctica, in *Geological Evolution of Antarctica*, edited by M. R. A. Thompson et al., pp. 345–351, Cambridge Univ. Press, Cambridge, Mass.

Weaver, S., C. Adams, R. Pankhurst, and I. Gibson (1992), Granites of Edward VII Peninsula, Marie Byrd Land: Anorogenic magmatism related to Antarctic-New Zealand rifting, *Earth Environ. Sci. Trans. R. Soc. Edinb.*, *83*(1–2), 281–290, doi:10.1017/S0263593300007963.

Weaver, S. D., B. C. Storey, R. J. Pankhurst, S. B. Mukasa, V. J. DiVenere, and J. D. Bradshaw (1994), Antarctica-New Zealand rifting and Marie Byrd Land lithospheric magmatism linked to ridge subduction and mantle plume activity, *Geology*, *22*(9), 811–814, doi:10.1130/0091-7613(1994)022 < 0811:ANZRAM>2.3.CO;2.

Yakymchuk, C., C. R. Brown, M. Brown, C. S. Siddoway, C. M. Fanning, and F. J. Korhonen (2015), Paleozoic evolution of western Marie Byrd Land, Antarctica, *Geol. Soc. Am. Bull.*, *127*, 1464–1484.